JCI The Journal of Clinical Investigation

Differential roles of FOXO transcription factors on insulin action in brown and white adipose tissue

Erica P. Homan, … , Jason K. Kim, C. Ronald Kahn

J Clin Invest. 2021. https://doi.org/10.1172/JCI143328.

Research In-Press Preview **Endocrinology** **Metabolism**

Graphical abstract

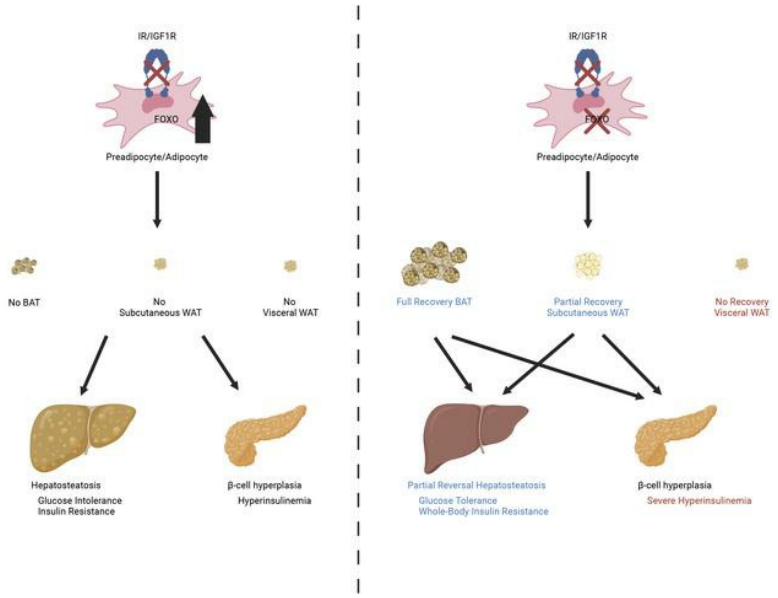

Differential Roles of FOXO Transcription Factors on Insulin Action in Brown and White Adipose Tissue

Erica P Homan[1,2], Bruna B Brandão[1], Samir Softic[1,3], Abdelfattah El Ouaamari[4,5,6], Brian T O'Neill[1,7], Rohit N. Kulkarni[4], Jason K. Kim[8,9], C. Ronald Kahn[1]

Affiliations:

[1] Section on Integrative Physiology and Metabolism, Joslin Diabetes Center, Harvard Medical School, Boston, MA

[2]Biology Department, Northeastern University, Boston, MA

[3]Division of Gastroenterology, Hepatology and Nutrition, Department of Pediatrics, and Department of Pharmacology and Nutritional Sciences, University of Kentucky College of Medicine, University of Kentucky, Lexington, KY.

[4] Section on Islet Cell and Regenerative Biology, Joslin Diabetes Center, Harvard Medical School, Boston, MA

[5] Department of Medicine, Division of Endocrinology, Metabolism and Nutrition, Robert Wood Johnson Medical School, Rutgers, The State University of New Jersey, New Brunswick, NJ, USA

[6]The Child Health Institute of New Jersey, Robert Wood Johnson Medical School, Rutgers, The State University of New Jersey, New Brunswick, NJ, USA

[7] Fraternal Order of Eagles Diabetes Research Center and Division of Endocrinology and Metabolism, Roy J. and Lucille A. Carver College of Medicine, University of Iowa, Iowa City, IA

[8] Program in Molecular Medicine, and [9]Division of Endocrinology, Metabolism and Diabetes, Department of Medicine, University of Massachusetts Medical School, Worcester, MA, USA

Address correspondence to:
C. Ronald Kahn, MD
Joslin Diabetes Center
One Joslin Place
Boston, MA 02215
Phone: (617)732-2635
Fax: (617)732-2487
Email: c.ronald.kahn@joslin.harvard.edu

Keywords: Insulin receptor, IGF-1 receptor, FoxO transcription factors, brown adipose tissue, white adipose tissue, lipodystrophy, β-cell hyperplasia, insulin resistance

Conflict of Interest: The authors have declared that no conflict of interest exists.

Abstract

Insulin and IGF-1 are essential for adipocyte differentiation and function. Mice lacking insulin and IGF-1 receptors in fat (FIGIRKO) exhibit complete loss of white and brown fat (WAT/BAT), glucose intolerance, insulin resistance, hepatosteatosis, and cold intolerance. To determine the role of FOXO transcription factors in the altered adipose phenotype, we generated FIGIRKO mice with fat-specific knockout of fat-expressed *Foxos* [*Foxo1*, *Foxo3*, *Foxo4*] (F-Quint KO). Unlike FIGIRKO mice, F-Quint KO mice had normal BAT, glucose tolerance, insulin-regulated hepatic glucose production, and cold tolerance. However, loss of FOXOs only partially rescued subcutaneous WAT and hepatosteatosis, did not rescue perigonadal WAT, or systemic insulin resistance, and led to even more marked hyperinsulinemia. Thus, FOXOs play different roles in insulin/IGF1 action in different adipose depots, being more important in BAT > subcutaneous WAT > visceral WAT. Disruption of FOXOs in fat also leads to a reversal of insulin resistance in liver, but not in skeletal muscle, and an exacerbation of hyperinsulinemia. Thus, adipose FOXOs play a unique role in regulating crosstalk between adipose depots, liver and β-cells.

Introduction

Insulin and IGF-1, acting through the insulin receptor (IR) and IGF-1 receptor (IGF1R), are critical hormones in the regulation of metabolism and growth (1). Following ligand binding, these receptors become autophosphorylated and recruit and phosphorylate substrate/adaptor proteins, such as IRS1, IRS2 and SHC (2). SHC activates the Ras-MAPK pathway, ultimately leading to increased cell proliferation, while the IRS proteins link to the PI3K-AKT pathway, leading to the regulation of multiple metabolic pathways including inhibiting gluconeogenesis and apoptosis, while stimulating glucose transport, glycogen synthesis, protein synthesis, gene transcription, and lipid synthesis (2).

In adipose tissue, insulin and IGF-1 are critical for differentiation of preadipocytes, and insulin facilitates glucose uptake and lipid synthesis while inhibiting lipolysis (3). Mice with genetic knockout of IR and IGF1R display a near complete loss of brown and white adipose tissues throughout life (4). As a result, these mice are unable to maintain their body temperature in the cold, accumulate ectopic lipid in both liver and muscle, and develop severe insulin resistance, glucose intolerance and pancreatic islet hyperplasia (4, 5). Likewise, inducible deletion of IR and IGF-1R in adipocytes results in the rapid loss of both white and brown fat due to increased lipolysis and increased adipocyte apoptosis (6). These observations demonstrated that insulin and IGF-1 signaling play a crucial role in both development and maintenance of brown and white adipose tissue.

One function of insulin/IGF-1 action, mediated via AKT, is the phosphorylation of members of the Forkhead box O (FOXO) family of transcription factors (7). When phosphorylated, FOXOs interact with the 14-3-3 proteins, leading to their exclusion from the

nucleus, thus blocking FOXO-mediated activation of programs governing gluconeogenesis and lipid synthesis (8-10). In the absence of IR/IGF1R or their ligands, FOXOs accumulate in the nucleus and remain active (7). In liver and muscle, reversing this activation by deletion of *Foxos* can reverse many of the phenotypes observed in mice lacking IR, IGF1R or their ligands. For example, mice lacking the IR in liver develop severe hepatic insulin resistance with unsuppressed hepatic glucose production leading to hyperglycemia, hyperinsulinemia, and glucose intolerance (11). Hepatic deletion of *Foxo1* in these mice rescues the insulin resistance and unsuppressed gluconeogenesis (12). Similarly, mice lacking both IR and IGF-1R in muscle or with insulin-deficient diabetes displayed a marked reduction in muscle mass due to increased proteasomal and autophagy-mediated protein degradation (13). Deletion of the muscle expressed *Foxos* in the context of lost IR/IGF-1R or insulin-deficient diabetes leads to normalization of autophagy and a rescue in muscle mass (14, 15). Thus, constitutive activation of FOXOs as a result of loss of insulin and/or IGF-1 signaling explains many of the metabolic abnormalities.

In the present study, we have explored the role of FOXOs in insulin/IGF-1 action in adipose tissue by determining the effect of fat-specific deletion of the adipose tissue-expressed *Foxos* (*Foxo1*, *Foxo3*, and *Foxo4*) in combination with deletion of IR and IGF1R. This reveals a differential role of these transcription factors in maintenance of different white and brown fat depots. This also uncovers unique roles of different fat depots in the crosstalk with the liver and in the marked hyperinsulinemia associated with lipodystrophy pointing to previously unrecognized differential mechanisms of adipose tissue-mediated regulation of systemic metabolism.

Results

Role of IR and IGF1R in Adipose Development and Partial Reversal by Deletion of *Foxo1/3/4*

We have previously reported that mice with fat specific knockout of IR and IGF1R have marked lipodystrophy with no detectable white fat and minimal amounts of brown adipose tissue (4). To address the role of downstream FOXO proteins in this phenotype, fat-specific *Insr*, *Igf1r*, as well as *Foxo1*, *Foxo3*, and *Foxo4* quintuple knockout mice (F-Quint KO) were generated using a Cre-recombinase transgene driven by the adiponectin promoter. F-Quint KO mice were compared with control floxed littermates [CONT] and with new cohorts of fat-specific *Insr* and *Igf1r* double knockout (FIGIRKO) mice. At 4-weeks of age, CONT mice weighed 16.1±0.5g, while FIGIRKO mice weighed only 13.3±0.9g, reflecting a decrease in fat mass **(Suppl Fig. 1A, $p<0.05$)**. By contrast, the weight of F-Quint KO mice was similar to CONT (16.8±0.4g) **(Suppl Fig. 1A)**. From weeks 5 to 9, FIGIRKO mice steadily gained weight surpassing the controls. This reflected both linear growth and increasing hepatomegaly (see below) **(Suppl Fig. 1A, $p<0.05$)**. Indeed, despite the absence of all white and most brown fat, DEXA analysis revealed similar total body fat in FIGIRKO mice relative to CONT **(Suppl Fig. 1B)** due to presence of fatty liver, consistent with previous studies (5). In contrast, F-Quint KO mice were similar in weight to CONT at 4 weeks of age and grew on a parallel track **(Suppl Fig. 1A, $p<0.05$)** but had a 68% reduction in fat relative to CONT ($p<0.01$) and FIGRKO ($p<0.01$) mice by DEXA **(Suppl Fig. 1B)**. Both FIGIRKO and F-Quint KO mice had about a 30% increase in lean mass relative to CONT mice **(Suppl Fig. 1C, $p<0.0001$)**.

At sacrifice at 12 weeks of age, FIGIRKO mice had no detectable perigonadal or inguinal (respectively representative of visceral and subcutaneous) white adipose tissue (WAT) and

minimal brown adipose tissue (BAT) **(Fig. 1A, B, and C)**. There was also a complete absence of visceral WAT in the F-Quint KO mice **(Fig 1A, p<0.0001)**, but unlike the FIGIRKO mice, there was a recovery in the mass of the subcutaneous WAT to about 30% of normal levels **(Fig 1B, p<0.05)** and full recovery in the mass of the BAT **(Fig 1C)**. Histologically, the recovered subcutaneous WAT in the F-Quint KO mice was similar in appearance to CONT littermates but did have an ~36% decrease in average adipocyte area and a modest increase in lymphocyte infiltration **(Fig 1D and Fig 1E)**. The brown adipose tissue in F-Quint KO contained a mixture of characteristic brown adipocytes with multilocular lipid droplets and brown adipocytes with larger unilocular fat droplets when compared with those in control littermates **(Fig 1F)**. This brown fat was functional as it restored normal cold-induced thermogenesis. Indeed, in contrast to the FIGIRKO mice, which failed to maintain their body temperature and dropped to 26.5°C by the end of the 5-hour cold exposure at 6°C, the F-Quint KO mice maintained their body temperatures similar to CONT during cold challenge **(Fig 1G)**.

To assess differences in differentiation capacity, white preadipocytes were isolated from the stromovascular fraction of subcutaneous WAT of control, double-floxed and quintuple-floxed mice and subjected to adenoviral-Cre mediated recombination in vitro to generate preadipocytes lacking *the Insr* and *Igf1r* (DKO) and preadipocytes lacking *Insr, Igf1r, Foxo1, Foxo3,* and *Foxo4* (QKO). Mirroring the *in vivo* observations, DKO subcutaneous white preadipocytes failed to differentiate and accumulate lipid, while both CONT and QKO subcutaneous white preadipocytes differentiated normally and showed equal lipid accumulation by Oil Red O staining **(Fig 1H)**. Assessment of the late adipogenic transcriptional markers, peroxisome proliferator activated receptor gamma (*Pparg*) and CCAAT enhancer-

binding protein alpha (*Cebpa*) by RT-qPCR of cells isolated after 4 days of differentiation confirmed 97% and 73% reductions in expression in DKO cells relative to CONT respectively **(Fig S2A)**. The expression levels of both *Pparg* and *Cebpa* were fully restored with loss of Foxos in the QKO cells **(Fig S2A)**. This was associated with a 1.7-fold increase in isoproterenol induced lipolysis in DKO cells relative to WT, and this was normalized in QKO cells **(Fig S2B)**. In contrast, the normal increase in insulin-mediated glucose uptake observed in CONT cells was not observed in DKO and QKO cells **(Fig S2C)**.

Recovery of glucose homeostasis but worsening of hyperinsulinemia in F-Quint KO mice

Assessment of glucose homeostasis at 12 weeks of age revealed marked hyperglycemia in FIGIRKO mice (fed glucose 466±33 vs 177±5 mg/dl) which were reduced to near control levels (213±16 mg/dl) in the F-Quint KO mice **(Fig 2A)**. Similar changes were seen in the fasted state **(Fig 2A)**. An intraperitoneal (i.p.) glucose challenge revealed markedly impaired glucose tolerance in FIGIRKO mice at all time points, while glucose tolerance in F-Quint KO mice was similar to controls **(Fig 2B)**. Consistent with severe insulin resistance, fed insulin levels were elevated 25-fold in FIGIRKO mice compared to controls **(Fig 2C, $p<0.0001$)**. Surprisingly, the hyperinsulinemia worsened in the F-Quint KO mice, with a 75-fold increase in insulin levels compared to controls **(Fig 2C, $p<0.0001$)**. This order of insulin levels persisted in the fasted state with F-Quint KO > FIGIRKO > CONT **(Fig 2C)**.

To determine whether the increase in serum insulin levels was due to increased secretion versus altered clearance, we assessed C-peptide levels. Like the serum insulin levels, C-peptide levels in F-Quint KO were four-fold higher than the FIGIRKO mice in the fed state ($p<0.0001$) and almost two-times higher in the fasted state ($p<0.05$), indicating increased

insulin secretion **(Fig 2D)**. Insulin resistance, as estimated by the HOMA-IR revealed that both the FIGIRKO and F-Quint KO mice were markedly insulin resistant **(Fig 2E, $p<0.0001$ and $p<0.001$, respectively),** and this was confirmed by an insulin tolerance test (ITT). FIGIRKO mice were markedly hyperglycemic compared to controls at the start of the ITT and failed to respond to insulin at all time points **(Fig 2F, $p<0.05$)**. F-Quint KO mice, on the other hand, started the ITT at similar glucose levels as controls, but like FIGIRKO mice failed to respond to insulin **(Fig 2F, $p<0.05$)**. These data indicate that while the loss of *Foxos* in fat can reverse the hyperglycemia observed in the FIGIRKO mice, the F-Quint KO mice remain severely insulin resistant and hyperinsulinemic.

β-Cell hyperplasia persists in F-Quint KO mice

Consistent with the elevated serum levels of insulin and C-peptide, histological examination revealed β-cell hyperplasia in both FIGIRKO and F-Quint KO mice relative to CONT **(Fig 3A)** with a 4.3-fold increase in islet mass in FIGIRKO mice and a 5-fold increase in F-Quint KO mice **(Fig 3B, $p<0.05$)**. This was associated with a 3-fold increase in the percentage of proliferating (Ki67 positive) β cells in both FIGIRKO and F-Quint KO mice as compared with controls **(Fig 3 A, C, $p<0.05$)**. An *in vivo* glucose-stimulated insulin secretion assay at 6 months of age showed low, but normal, glucose-stimulated insulin secretion in controls, whereas in FIGIRKO mice, basal insulin levels were modestly elevated, and there was a more robust first and second phase insulin release **(Suppl Fig. 3A, $p<0.05$)**. F-Quint KO mice showed even more marked increases in basal insulin levels which persisted throughout the glucose stimulation test **(Suppl Fig. 3A, $p<0.05$)**. Exposure to 16.7 mM glucose produced about a two-fold increase in

insulin secretion in an *in vitro* GSIS carried out on islets isolated from 2-month-old CONT mice. This was increased to a 4.8-fold stimulation of insulin secretion in FIGIRKO islets and further enhanced in F-Quint KO islets to greater than a 9.3-fold increase **(Fig 3D).** Although elevated circulating C-peptide indicated increased insulin secretion, the ratio of serum C-peptide to insulin in the fed state was reduced by 50% in FIGIRKO and F-Quint KO mice ($p<0.01$ and $p<0.05$, respectively), indicating that reduced insulin clearance may also contribute to the elevation in circulating insulin **(Suppl Fig. 3B)**. In contrast, in the fasted state there was 2.5-fold increase in the C-peptide:insulin ratio in FIGIRKO mice relative to CONT, and this ratio was further increased to 3.8-fold in F-Quint KO mice, indicating increased insulin clearance may contribute to the lower circulating insulin levels in the fasted state **(Suppl Fig. 3B, $p<0.001$)**. SERPINB1 is a circulating serine protease inhibitor produced mainly in liver and has been previously shown to contribute to increased β-cell proliferation in mice with insulin resistance (16). Although there was no difference in the hepatic expression of *Serpinb1* or in fasted serum SERPINB1 levels between CONT and FIGIRKO mice, we observed a significant 2-fold increase in serum SERPINB1 protein levels in F-Quint KO mice as compared with CONT suggesting that SERPINB1 may contribute to the islet hyperplasia observed in these mice **(Fig 3E, Suppl Fig. 3C-F, $p<0.01$)**.

Partial recovery of serum triglycerides, free fatty acids, and adipokine levels in F-Quint KO mice

Consistent with their lipodystrophic phenotype (5), there was a significant increase in serum triglycerides in FIGIRKO mice in both the fed (12.3-fold, $p<0.0001$) and fasted (2.6-fold,

p<0.05) states **(Fig 4A)**. Deletion of *Foxos* largely rescued this hypertriglyceridemia despite persistent partial lipodystrophy **(Fig 4A)**. There was also a significant increase in serum free fatty acids (FFAs) in the FIGIRKO mice in the fed state, which was significantly improved in the F-Quint KO mice, although serum FFAs remained about 2-fold elevated compared to CONT **(Fig 4B, p<0.05)**. In both the fed and fasting state, there was a marked decrease in adiponectin levels in the FIGIRKO mice, and this recovered to about 20% of normal levels in the F-Quint KO mice, paralleling the partial recovery of subcutaneous WAT **(Fig 4C, p<0.0001)**. In the fed state, leptin levels were reduced by ~71% and 53% in the FIGIRKO and F-Quint KO mice, respectively **(Fig 4D, p<0.0001)**. This was also true for FIGIRKO mice in the fasted state, whereas fasted F-Quint KO mice had leptin levels similar to controls **(Fig 4D, p<0.001)**.

Improved food and water intake and fasted energy expenditure in F-Quint KO mice

Consistent with decreased levels of circulating leptin and diabetic phenotype, FIGIRKO mice were hyperphagic compared with CONT with more than a doubling of food intake **(Fig 5A)** and a parallel increase in water consumption (**Fig 5B**). Both of these phenotypes were partially rescued in the F-Quint KO mice **(Fig 5A**, **5B)**. Energy expenditure assessed using Comprehensive Lab Animal Monitoring Systems (CLAMS) metabolic cages in CONT mice revealed a normal fed-fasted pattern of respiratory exchange ratio (RER), being about 0.9 in the fed state, indicating preferential utilization of carbohydrates, and falling to about 0.7 in the fasted state, consistent with high levels of fat oxidation. This pattern was completely lost in FIGIRKO which had stable RER of 0.75-0.8 throughout the fed and fasted period **(Fig 5C)**. F-Quint KO mice had low RER in the fed state (p<0.001), but this dropped during fasting in a manner similar to wildtype mice

(Fig 5C). These differences in RER related to differences in both O_2 consumption and CO_2 production in both FIGIRKO and F-Quint KO mice **(Suppl Fig. 4A, B)**.

Partial rescue of hepatosteatosis with loss of *Foxo1/3/4*

We have previously shown that FIGIRKO mice develop severe hepatosteatosis due to their inability to store fat in adipose tissue (5). In the present study, average liver weight in FIGIRKO mice was 5.7±0.2g, which was almost seven-fold increased over controls (0.85±0.03g) **(Fig 6A, p<0.0001)**. This was associated with a 3.1-fold increase in hepatic triglyceride content **(Fig 6B, p<0.0001)**. Histologically, FIGIRKO livers exhibited micro- and macro-vesicular steatosis throughout the liver **(Fig 6C)**. By comparison to FIGIRKO, liver weights of the F-Quint KO mice were reduced by 55% but were still 3-fold greater than that of controls **(Fig 6A, p<0.0001)**. In F-Quint KOs, there was a proportional decrease in triglyceride content and reduction in steatosis histologically **(Fig 6B, C, p<0.0001)**.

These histological changes in liver were associated with changes in the expression of gluconeogenic and lipogenic enzymes and markers of inflammation and fibrosis. Thus, there was a 2-fold increase in the expression of glucose-6-phosphatase catalytic subunit (*G6pc*) in livers of the FIGIRKO mouse, which was reduced in the F-Quint KO mice to below CONT levels **(Fig 6d, p<0.0001)**. Similarly, expression of phosphoenolpyruvate carboxykinase 1 (*Pck1*) and fructose-bisphosphatase 1 (*Fbp1*) were increased in FIGIRKO livers by 1.6- and 2.3-fold, respectively, and were restored to CONT levels in the F-Quint KO livers **(Fig 6D)**. Interestingly, there was also a 2.1-fold increase in expression of pyruvate carboxylase (*Pc*) in FIGIRKO liver, however, deletion of *Foxos* did not rescue this change **(Fig 6D, p<0.01)**. Also, deletion of *Foxos*

did not rescue the increased expression of fatty acid synthase (*Fasn*) and stearoyl-CoA desaturase 1 (*Scd1*) observed in FIGIRKO mice **(Fig 6D)**. Although there was no difference in expression of acetyl-CoA carboxylase alpha (*Acaca*) or tumor necrosis factor-α (*Tnf-*α) among the three groups, there was a 12-fold increase in the expression of the inflammation marker integrin alpha X (*Itgax*) in FIGIRKO livers ($p<0.0001$), which was rescued in the F-Quint KO mice **(Fig 6D)**. FIGIRKO livers also displayed increases in expression of transforming growth factor beta 1 (*Tgfb1*) ($p<0.0001$), alpha 1 chain of type I collagen (*Col1a1*) ($p<0.01$), and actin, alpha 1, skeletal muscle (*Acta1*) ($p<0.0001$) when compared with CONT livers, which were rescued in the F-Quint KOs **(Fig 6D)**.

Restoration of liver insulin signaling in F-Quint KO mice

To determine the potential mechanism of the improved metabolic state in F-Quint KO mice, we assessed liver and muscle insulin sensitivity by *in vivo* stimulation. In both the basal and stimulated state, there was a 4-fold decrease in the level of IR protein in livers of FIGIRKO mice relative to CONT ($p<0.0001$), and this was partially recovered in the F-Quint KO mice ($p<0.001$) **(Fig 7A, B).** Despite the decrease in receptor content, there was a 3-fold increase in the absolute level of basal phosphorylation of the insulin receptor (pIR) in FIGIRKO mice relative to control, resulting in a 15-fold increase in the ratio of phospho-IR to IR **(Fig 7A-D, p<0.0001)**. Response to exogenous insulin, however, was markedly blunted due to down regulation of the receptor. In the F-Quint KO mice, the increase in basal IR phosphorylation persisted, but there was a more robust increase in the insulin-stimulated phosphorylation and a partial recovery in the level of IR protein resulting in normalization of the ratio of pIR to IR when

insulin stimulated, whereas basal IR phosphorylation relative to IR protein remained elevated **(Fig 7A-D)**. A similar increase in basal insulin signaling was observed by increased pAKT/AKT in FIGIRKO and F-Quint KO mice relative to control **(Fig 7A, E)**, and following insulin stimulation, there was an increase in pAKT/AKT in F-Quint KO livers relative to control and FIGIRKO livers **(Fig 7A, E)**. We did not observe any differences in basal or stimulated phosphorylation of ERK1/2 or total ERK1/2 among the three groups **(Fig 7A, F)**, but there was a significant 2-fold increase in Grb2 protein in the F-Quint KO liver **(Fig 7A, G, $p<0.001$)**. There was no difference in the expression of *Insr* mRNA in CONT, FIGIRKO and F-Quint KO liver **(Fig S5A)**.

As in liver, insulin signaling in muscle revealed insulin resistance in FIGIRKO mice, but in this case, there was no recovery in the F-Quint KO mice. In contrast to the robust increase in phospho-IR in CONT mice following insulin stimulation ($p<0.0001$), we observed no increase in insulin-stimulated IR phosphorylation in either FIGIRKO and F-Quint KO muscle **(Fig 7H, J)**, and there was no significant change in total IR protein levels **(Fig 7H, I)**. There was also no significant change in phosphorylation of AKT or ERK1/2 in response to insulin in FIGIRKO muscle **(Fig 7H, L, M)**. Although there was a recovery in insulin-stimulated phosphorylation of AKT, we observed no recovery in the phosphorylation of ERK1/2 in F-Quint KO mice **(Fig 7H, L, M, $p<0.0001$),** and Grb2 protein levels were unchanged **(Fig 7H, N)**.

To determine the physiological effect of these changes, we performed hyperinsulinemic-euglycemic clamp in awake mice **(Suppl Fig. 5B)**. Relative to CONT, both FIGIRKO and F-Quint KO mice were whole-body insulin resistant as demonstrated by a 75% reduction in the glucose infusion rate during the clamp **(Fig 8A, $p<0.05$)**. This occurred despite the fact that insulin levels obtained during the clamp were 2-fold higher in FIGIRKO and F-Quint KO mice as

compared to CONT, consistent with decreased insulin clearance in these mice **(Suppl Fig. 5C)**. Based on tracer infusion, whole body glucose turnover rates were reduced by 40% in FIGIRKO mice compared to CONT, and this worsened to a 60% decrease in F-Quint KO mice **(Fig 8B, p<0.0001)**. Similarly, whole body glycolysis was decreased by 67% in FIGIRKO mice relative to CONT ($p<0.01$) and was reduced further in F-Quint KO mice ($p<0.0001$) **(Suppl Fig. 5D)**. Relative to CONT, there was also a 50% decrease in whole body glycogen plus lipid synthesis in both the FIGIRKO and F-Quint KO mice **(Fig 8C, p<0.01)**. Assessment of glycogen synthase kinase-3 (GSK3) levels in liver revealed a significant 1.3-fold increase in GSK3 levels in FIGIRKO relative to CONT **(Fig S6A, C).** No significant difference was detected in GSK3 levels in the livers of F-Quint KO mice relative to either CONT and FIGIRKO **(Fig S6A, C)**. Expression of the downstream target of GSK3, *glycogen synthase 2 (Gys2)* in liver was reduced by ~50% in FIGIRKO relative to CONT, and this was fully recovered in F-Quint KO **(Fig S6E).** Assessment of GSK3 levels in muscle did not reveal any differences between genotypes **(Fig S6B, D).** There was no difference in insulin-stimulated glucose uptake in skeletal muscle between CONT and FIGIRKO mice, but this was significantly reduced by 85% in F-Quint KO mice **(Fig 8D, p<0.01)**. Systemic insulin resistance was also reflected by a 2-fold increase in basal hepatic glucose production in the FIGIRKO mice and a failure to suppress hepatic glucose production (HGP) during the insulin clamp; both of these parameters reverted toward normal in the F-Quint KO mice **(Fig 8E)**. Hepatic insulin action, calculated as insulin-mediated percent suppression of basal HGP, showed a 70% reduction in FIGIRKO mice relative to control, and this was rescued in the F-Quint KO mice **(Fig 8F, p<0.0001)**. Taken together, the clamp data indicate severe insulin resistance in muscle and

liver of FIGIRKO mice. In F-Quint KO mice, insulin resistance in liver, but not in skeletal muscle, was selectively reversed.

Discussion

FOXO transcription factors play important roles in insulin action (17). Following insulin stimulation, FOXOs are phosphorylated, bind to 14-3-3 proteins and retained in the cytoplasm, while in the absence of insulin/IGF-1 signaling, they are localized in the nucleus where they are constitutively active (8, 9). In mice lacking insulin and IGF-1 receptors in liver or muscle, tissue specific deletion of *Foxos* can reverse many of the effects of receptor loss at the transcriptional level (12, 14). In the present study, we assessed to what extent deletion of *Foxos* could reverse the lipodystrophic phenotype observed in mice lacking IR and IGF1R in fat (FIGIRKO mice) and how this might provide new insights into tissue communication in the altered metabolism of lipodystrophy. We find that deletion of *Foxos* in the context of absent IR and IGF1R fully restores BAT mass, allows mice to adapt to a cold challenge, and partially restores subcutaneous WAT resulting in improved hepatosteatosis and liver insulin sensitivity. However, deletion of *Foxos* has no effect on restoring visceral WAT, does not reverse muscle insulin resistance and actually exacerbates the severe hyperinsulinemia observed in FIGIRKO mice. This divergence of rescue effects points to different roles of FOXO proteins in different adipose depots and how each of these depots contributes to the different phenotypes associated with lipodystrophy.

FOXO proteins were first recognized as downstream insulin/IGF-1 signaling in C. elegans, such that deletion of Daf-16 (the FOXO homologue) was able to reverse the longevity phenotype observed in worms lacking Daf-2 (the IR/IGF1R homologue) (18). In mice, liver specific deletion of the insulin receptor leads to a wide range of changes in gene expression, increased hepatic glucose production and hyperglycemia, and these are largely rescued by

deletion of *Foxo1*, the major FOXO protein in the liver (11, 12). Likewise, the major phenotype of muscle-specific deletion of *Insr* and *Igf1r* in mice is a loss in muscle mass due to increased autophagy-lysosomal degradation and is largely rescued by *Foxo* deletion (13, 14). In this tissue, however, rescue requires deletion of *Foxo-1, -3* and *-4*, since muscle expresses these three FOXO proteins with overlapping functions (14). Also, in this tissue, deletion of *Foxos* was not sufficient to rescue the abnormal proteasomal activity nor the abnormality in insulin-stimulated glucose transport following receptor deletion (14). Adipose tissue shows even more complexity, since it depends not only on three FOXO proteins, but also the biology of adipose tissue differs greatly from one fat depot to another (19). Thus, creation of an F-Quint KO mouse, completely rescues brown fat mass and function, partially corrects the loss of subcutaneous white fat, but has virtually no effect on rescuing visceral WAT and some of its functions.

Previous studies have shown that a major role of FOXO1 in fat is to suppress adipogenesis (20). Using the 3T3-F442A preadipocyte cell line, Nakae et. al. found that FOXO1 binds to the promoter of *Pparg* and inhibits its expression (20). Additionally, through its interaction with PPARγ, FOXO1 blocks the formation of the PPARγ/RXR functional complex involved in adipogenesis (21). In preadipocytes lacking IR, IRS proteins, or AKT, there is an increase in FOXO1 activation coupled with impaired differentiation (22). Nakae et. al. found that expressing a dominant-negative form of FOXO1 is sufficient to restore adipocyte differentiation from insulin receptor knockout embryonic fibroblasts (20). In vitro, we find that knockout of *Foxo-1, -3* and *-4* is also able to allow recovery of differentiation in immortalized subcutaneous white preadipocytes derived from mice with knockout of *Insr* and *Igf1r* as

demonstrated by the recovery of both Oil RedO staining and expression of the late adipogenic markers (*Pparg* and *Cebpa*). This is consistent with the partial recovery of subcutaneous WAT and full recovery of BAT *in vivo*. But this does not explain why there is only partial recovery of subcutaneous WAT and no recovery in visceral WAT in the F-Quint mice. Clearly, there must be other insulin-regulated, but FOXO-independent factors required for normal preadipocyte differentiation in these depots. In addition to FOXOs ability to suppress adipocyte differentiation, previous work has shown that FOXOs suppress lipogenesis in WAT in part by suppressing PEPCK expression and glycerologenesis, both of which facilitate triglyceride formation (23). One factor may be the effect of loss of IR/IGF1R on the ability of insulin to suppress lipolysis, where overactive FOXOs promote lipolysis by promoting adipose triglyceride lipase expression (24). Loss of FOXOs in F-Quint KO mice may also help promote the ability to form and store triglycerides in WAT. A recovery in lipolysis is observed in the QKO cells, indicating the WAT that does recover is functional. This is also consistent with the partial restoration of FFA and reduced adipocyte cell size observed in F-Quint KO mice in the fed state relative to FIGIRKO and CONT mice.

Although still incompletely understood, recent publications have identified heterogeneity of white adipocytes, both between visceral and subcutaneous adipose depots and even within a single depot (25-28) . These different types of white adipocytes exhibit notable differences in the receptor density, affinity, and signal transduction, and also levels of expression of different transcription factors including FOXOs (26). In addition, visceral adipose tissues have high levels of glucocorticoid and androgen receptors (29), while subcutaneous adipocytes have higher estrogen receptor binding (30). Visceral WAT is also more sensitive to

catecholamine stimulated lipolysis than subcutaneous WAT due to an enrichment of β_3-adrenoreceptors, and differences in lipolysis have also been observed between white adipocyte subtypes (26). These differences in receptor signaling and receptor crosstalk can impact adipocyte differentiation in a depot specific manner and could serve as an explanation for only partial recovery of subcutaneous WAT and no recovery of visceral WAT in the F-Quint KO mice.

In addition to differences at the receptor level, there are notable differences in the expression of developmental genes in different WAT depots, with *Nr2f1, Gpc4, Thbd, HoxA5*, and *HoxC8* more highly expressed in visceral WAT and *Tbx15, Shox2, En1, Sfrp2*, and *HoxC9* more highly expressed in subcutaneous WAT (31). These developmental genes have been shown to play roles in adipocyte differentiation, triglyceride accumulation, and controlling lipolytic rate (31). Important differences have also been observed in the role of growth factors like BMP-2, BMP-4 and BMP-7 in white and brown preadipocyte differentiation (32, 33). One striking feature of this model is the almost complete recovery in BAT relative to the partial recovery of subcutaneous WAT and lack of recovery of visceral WAT. While these differences indicate differential roles of FoxOs in BAT than WAT development, it may also represent some effects of endocrine factors produced by WAT, such as leptin and adiponectin, on BAT versus WAT differentiation. Further experiments are needed to determine to what extent these and other factors account for the differences in adipocyte development in different depots in the F-Quint KO mice.

Another important difference between F-Quint KO and FIGIRKO mice is the improvement in hepatosteatosis, hepatic insulin sensitivity and glucose levels following deletion of *Foxos* in adipose tissue. Since the knockouts are all adipose tissue specific, these

effects must be secondary to either metabolic or hormonal crosstalk between fat and other tissues. Previous studies have shown that increasing the function and mass of subcutaneous adipose tissue via treatment with thiazolidinediones (TZDs) or genetic overexpression of adiponectin leads to decreased hepatosteatosis and increased insulin sensitivity, even in the face of obesity or type 2 diabetes (34). This has been mainly attributed to an increase in the ability of fat to store triglycerides, thus reducing hepatic fat accumulation (34). However, in our F-Quint KO model, there is only partial recovery in subcutaneous WAT mass and partial reversal of hepatic triglyceride accumulation, suggesting there must be other factors contributing to the organ-to-organ crosstalk and improvement in liver metabolism. These most likely represent a change in some adipose secreted hormones that affect hepatic insulin sensitivity (25).

In addition, recovery of BAT could also account for some improvement in glycemia and hepatosteatosis in F-Quint KO mice. In contrast to WAT, which functions to store excess energy, BAT oxidizes FFAs and glucose to produce heat and thus contributes to whole body glucose and fatty acid homeostasis (19). Indeed, increasing BAT mass by BAT transplantation to superphysiological levels can partially reverse the abnormal glucose tolerance observed in high fat diet-fed mice, even under conditions when it does not reduce the obesity (35). This positive effect was lost when BAT from Il6 knockout mice was utilized in the BAT transplantation, suggesting a role of this cytokine on glucose homeostasis and insulin sensitivity (36). BAT produced NRG4 has also been shown to improve obesity related insulin resistance (37). We demonstrated previously that BAT is also a major source of circulating exosomal miRNAs, which has the ability to affect metabolism in many target tissues, including liver (38). Thus, recovery

of BAT in the F-Quint KO mice could account for some of the decrease in serum FFAs, improvement in glucose homeostasis and hepatosteatosis.

Adiponectin is an adipokine involved in regulating glucose levels through its role in enhancing insulin sensitivity by increasing fatty acid oxidation and inhibiting hepatic glucose production (39, 40). While all adipose depots make adiponectin, most circulating adiponectin comes from subcutaneous WAT and marrow adipose tissue (41). The partial recovery in serum adiponectin levels observed in the F-Quint KO mice is likely due to the partial recovery of subcutaneous WAT and could contribute to the improvement in hepatic insulin sensitivity and normalization of hepatic gluconeogenic enzymes but is unlikely to be sufficient to account for the marked improvement observed in the F-Quint KO mice.

Another interesting aspect of the partial recovery of metabolic defects in the F-Quint KO is that despite a recovery in insulin signaling in liver, as evidenced by enhanced phosphorylation of IR, AKT, and ERK, in the F-Quint KO mice, there remains severely impaired insulin signaling in muscle of F-Quint KO mice, similar in level to that observed in FIGIRKO mice. This differential insulin resistance is also supported by the clamp data, where liver insulin sensitivity, i.e., the ability of insulin to turn off hepatic glucose production, is partially recovered in F-Quint KO mice. Mechanistically, this is also supported by reversal of the increase in the gluconeogenic enzymes, *G6pc, Pck1, Fbp1, and Pc,* observed in the F-Quint KO livers as compared to FIGIRKO livers. Despite the markedly improved glucose tolerance phenotype in the F-Quint KO mice, these mice remain insulin resistant in muscle as demonstrated by the low glucose infusion rates during the clamp and the decrease in skeletal muscle glucose uptake. Thus, it is likely that the markedly increased insulin secretion in the F-Quint KO mice and the partial recovery of hepatic

insulin action result in the improved glucose tolerance. The cause for the persistent low glucose uptake in skeletal muscle in F-Quint KO mice is unclear, since AKT phosphorylation, which plays a critical role in insulin-mediated glucose uptake (2), is recovered in the soleus muscle of F-QuintKO mice. While we did not directly assess PI3K activity, non-esterified fatty acids (NEFA) can induce a defect in muscle glucose due to impaired PI3K activation (42), and PI3K can also act through atypical PKCs and other mechanisms to facilitate glucose uptake (43, 44).

It is well established that insulin action decreases the lipolysis and release of NEFAs and glycerol from WAT and in turn, promotes gluconeogenesis via hepatic fatty acid oxidation (45). The recovery of some adipose tissue depots in F-Quint KO mice permits triglyceride storage in WAT, leading to lower free fatty acid levels in the in the serum. While insulin-mediated inhibition of lipolysis is likely still impaired in F-Quint KO mice, insulin could potentially suppress lipolysis indirectly via dampening of the central nervous system and the recovery of circulating serum leptin levels (46). Indeed, as noted above, it is possible that maintained lipolysis and elevated NEFAs and glycerol could contribute to the partial suppression of HGP observed in F-Quint KO mice.

An even more remarkable aspect of the F-Quint KO phenotype is the marked hyperinsulinemia in the mice as compared to both FIGIRKO and control mice. Hyperinsulinemia can be a result of increased insulin secretion and/or decreased insulin clearance (47). With the liver responsible for approximately ~80% of insulin clearance (48) and a clear improvement in hepatosteatosis, along with the reduced liver insulin resistance, in the F-Quint KO mice, one might predict a recovery in the decreased insulin clearance observed in the FIGIRKO mice in F-

Quint KO mice. However, insulin clearance, as determined by the ratio of C-peptide to insulin, remains decreased in F-Quint KO mice. Thus, insulin clearance does not account for the extraordinary hyperinsulinemia observed in the F-Quint KO mice. Instead, we found even more highly enhanced enhanced glucose-stimulated insulin secretion in the F-Quint KO mouse compared to the FIGIRKO mouse, which already has a significant increase in β-cell mass and insulin secretion. This occurs in spite of any potential effects of glucotoxicity and lipotoxicity on β-cell function (4, 49). What stimulates further β-cell hyperfunction in F-Quint KO mice is not clear, but identification of this factor will be of great interest. Previous work has demonstrated that hepatic insulin resistance due to liver specific knockout of the insulin receptor results in increased secretion of SERPINB1 and that this contributes to β-cell proliferation (16, 50). While F-Quint KO mice do have a modest increase in SERPINB1 compared to FIGIRKO mice, it seems unlikely that this could drive such a major increase in β-cell proliferation. It seems more likely that recovery in the brown and/or partial recovery of subcutaneous WAT allows for secretion of additional factors that influence pancreatic β-cell growth. It is also possible that some FOXO-dependent adipokine functions to suppress islet proliferation and/or insulin secretion and thus, loss of FOXOs in F-Quint KO mice reverses this suppression and lead to enhanced insulin secretion. As noted above, previous work from our lab has demonstrated that adipose tissue serves as an important source for circulating exosomal miRNAs and that these miRNAs can influence gene expression in other tissues (38). Thus, it is possible that with the recovery of BAT and partial recovery of subcutaneous WAT restore exosomal secretion of one or more miRNAs that have an impact on β-cell proliferation, insulin secretion, or peripheral glucose

metabolism. Future work identifying these factors are of high priority, since these could provide new approaches to the treatment of both type 1 and type 2 diabetes.

One limitation of this study is that the adiponectin Cre is developmentally expressed and therefore, the knock-out occurs in early development. Future experiments using an inducible adiponectin cre (6) for ablation of IR and IGF1R in combination with Foxo1/3/4 in adult mice could allow us to determine the kinetics of cross-talk between adipose tissue FOXOs and liver, pancreas, and glucose homeostasis.

In conclusion, loss of IR and IGF1R in adipose tissue results in severe lipodystrophy and a metabolic syndrome with insulin resistance, fatty liver, and increased circulating triglycerides and FFAs. Deletion of *Foxo-1, -3* and *-4* in adipose tissue of these mice results in the recovery of brown adipose tissue, a partial recovery of subcutaneous WAT, but has no effect on visceral WAT. Systemically, this is associated with a recovery in glucose homeostasis and thermogenesis, an improvement in hepatic insulin signaling and hepatosteatosis, but a lack of improvement in insulin sensitivity in muscle and a worsening of hyperinsulinemia. Thus, FOXO proteins play very different roles in white and brown adipose tissue development, and even between different white adipose depots. Their knockout uncovers a new level of crosstalk between fat and other tissues in which different adipose depots exert unique effects on systemic glucose metabolism and insulin resistance in muscle versus liver. More importantly, this also demonstrates unique crosstalk between adipose tissue and the β-cell response to insulin resistance opening a pathway for regulation of each of these processes in independent ways.

Methods

Animals, Diets, and Whole-body Energy Expenditure

Mice were housed at 20-22°C on a 12-h light/dark cycle with ad libitum access to water and food (Mouse Diet 9F; PharmaServ). The sources for the alleles used in this study: *Insr^{lox}(51), Igf1r^{lox}(52), Foxo1^{lox}(53), Foxo3^{lox}(54), Foxo4^{lox}(53)*. FIGIRKO or F-Quint KO mice were generated by breeding *Insr$^{lox/lox}$;Igf1r$^{lox/lox}$* mice or *Insr$^{lox/lox}$;Igf1r$^{lox/lox}$;Foxo1$^{lox/lox}$;Foxo3$^{lox/lox}$;Foxo4$^{lox/lox}$* mice on a C57Bl/6-129Sv genetic background, respectively, with mice carrying Cre recombinase driven by the adiponectin promoter (Adipo-Cre) on a C57Bl/6 background. Adipo-Cre-positive males and Adipo-Cre-negative female mice of each genotype were used for final breeding, and breeder pairs of each genotype were replaced simultaneously every 6 months to ensure that there is little or no genetic drift. Male mice were used throughout the study. Control mice from both double and quintuple floxed mice showed no physiological differences and were pooled into a single control group (CONT). A Comprehensive Lab Animal Monitoring System (Columbus Instruments) was used to measure whole-body energy expenditure (VO2, VCO2, food and water intake) at ambient temperature (~22°C).

Glucose and Insulin Tolerance Tests

Glucose tolerance tests were performed on overnight fasted mice by injection of dextrose (2mg/g) intraperitoneally, and blood glucose was measured at 0, 15, 30, 60, and 120 minutes using an Infinity glucose meter (US Diagnostics). Insulin tolerance tests were performed in 2h fasted mice by injection with insulin (1unit/kg i.p.; Humulin R; Lilly). Glucose levels were measured at 0, 15, 30, 60and 90 min post injection.

In Vivo Glucose-Stimulated Insulin Secretion (GSIS)

Mice were fasted overnight then injected intraperitoneally with dextrose (3mg/g body weight). Serum was collected at 0, 2, 5, 10, and 30 minutes, and insulin concentrations determined using an ultrasensitive mouse insulin ELISA kit following the low range protocol specified by the manufacturer (Crystal Chem Inc., catalog #90080).

In Vitro GSIS

In vitro glucose-stimulated insulin secretion (GSIS) was assessed as described (55). Briefly, approximately 5×10^5 β-cells were washed with Krebs ringer buffer (KRB - 128mM, NaCl, 5mM KCl, 2.7mM $CaCl_2$, 1.2mM $MgCl_2$, 1mM Na_2HPO_4, 1.2mM KH_2PO_4, 5mM $NaHCO_3$, 10mM HEPES and 0.1%BSA in deionized water), then incubated for 2 hours in 2mM glucose (Sigma) in KRB. After incubation, cells were sequentially incubated for 30 minutes each alternating 2 and 20 mM glucose in KRB then with 30 mM KCl in KRB. The supernatants after each 30-minute incubation were collected, and insulin was quantified using the Stellux rodent insulin ELISA kit (ALPCO Diagnostics).

Body Temperature and Cold Exposure

Body temperature was measured in 3-month-old mice using a RET-3 rectal probe (Physitemp). The mice were housed individually at an ambient temperature of 6°C, and the temperature was measured every 30 minutes for 3 hours or until the body temperature dropped below 25°C.

Tissue and Serum Analysis

Body and tissue weights were measured using a Sartorius BP610 Balance. Fed and fasting blood glucose levels were measured using an Infinity Glucose Meter (US Diagnostics). Fed and fasting blood was collected by cheek puncture, and serum was isolated using Microtainer SST tubes (BD) following the protocol recommended by the manufacturer. Fed and fasting insulin, leptin, C-peptide, TG, and FFA levels were determined by ultrasensitive mouse insulin ELISA (Crystal Chem Inc.), mouse leptin ELISA (Crystal Chem Inc.), Mouse C-Peptide ELISA (Crystal Chem Inc.), Free Fatty Acid Quantitation Kit (Sigma-Aldrich), respectively. Hormones and adipokines were assessed by ELISA. Triglycerides from liver samples were measured with a triglyceride quantification kit (Abnova) (56). Tissues were fixed in formalin, and sections were stained with hematoxylin and eosin (H&E). mRNA extraction and quantification was performed as previously described (57).

Measurement of β-Cell Proliferation, Islet Area, and β-Cell Mass

Pancreatic tissue was immunostained using anti-Ki67 (BD Biosciences) and anti-insulin (Abcam) antibodies. Ki67+ β-cells were visualized immunofluorescence microscopy and counted by a blinded observer (50). Insulin-positive cells colocalized with nuclear DAPI and Ki67 immunostaining were counted as proliferating β-cells. The percent β -cell area was determined by ImageJ software (National Institutes of Health) and calculated as insulin-positive area divided by total pancreas area. The β-cell mass was calculated as previously described by the product of the overall pancreas weight measured at sacrifice by the percent β-cells (11).

Subcutaneous preadipocyte isolation, culture, glucose uptake and lipolysis assays

Preadipocytes were isolated from newborn *Insr*$^{lox/lox}$*;Igf1r*$^{lox/lox}$ mice or *Insr*$^{lox/lox}$*;Igf1r*$^{lox/lox}$*;Foxo1*$^{lox/lox}$*;Foxo3*$^{lox/lox}$*;Foxo4*$^{lox/lox}$ mice by collagenase digestion of subcutaneous WAT and immortalized by infection with retrovirus encoding SV40 T-antigen followed by the selection with 2 μg/ml hygromycin. Immortalized preadipocytes were infected with adenovirus containing GFP to generate a control cell line or GFP-tagged Cre recombinase to generate *Insr/Igf1r* double knockout (DKO) or *Insr/Igf1r/Foxo1/Foxo3/Foxo4* quintuple knockout (QKO) cell lines. GFP-positive cells were sorted by FACS and expanded in DMEM supplemented with 10% heat-inactivated fetal bovine serum (FBS, Sigma), 100 U ml^{-1} penicillin and 100 μg ml^{-1} streptomycin (Gibco) at 37 °C in a 5% CO_2 incubator. Oil Red O staining was performed as previously described (58). mRNA extraction and quantification were performed as previously described (26). For lipolysis, 9 days post-induction of differentiation, cells were starved for 4 hours in KRPHA buffer at 37C with shaking. After collecting media to measure basal glycerol release, cells were incubated in fresh KRPHA media containing 10μM isoproterenol for 90 minutes at 37^{o}C before media was collected to assess glycerol release using a colorimetric assay (26). For assessment of glucose uptake, 9 days post-induction of differentiation, adipocytes were serum deprived in DMEM supplemented with 0.25% BSA overnight and then starved in KRBH buffer for 1 hour at 37C. Cells were incubated in fresh KRBH buffer with or without 100nM insulin for 30 minutes before initiation with the addition of 1μDi/ml of ^{14}C-Deoxy-D-glucose for 10 minutes. The reaction was stopped by the addition of unlabeled 200mM 2-Deoxy-D-glucose. After 3 washes with ice cold PBS, cells were collected, protein concentration quantified and counts of ^{14}C-D-glucose asses after cell lysis in RIPA buffer.

***In Vivo* Insulin Stimulation**

Mice were fasted overnight (16 h) and recombinant human insulin (100IU/mL, 50μL; Humulin R) or saline was injected via the inferior vena cava after anesthesia with Avertin (150mg/kg i.p.). At 10 minutes post injection, soleus muscle, and liver were collected and flash frozen using liquid nitrogen.

Protein Extraction and Immunoblot Analysis

Tissues were homogenized in radioimmunoprecipitation assay buffer (EMD Millipore) with protease and phosphatase inhibitor cocktail (BioTools). Proteins were separated using SDS-PAGE and transferred to polyvinylidene difluoride membrane (Millipore). Immunoblotting was performed using the indicated antibodies: phosphorylated pIR (Tyr1135/1136)/IGFR (Tyr1150/1151) (Cell Signaling Technologies, #3024), total IR-β (Cell Signaling Technologies, #3020), pAKT (Ser473) (Cell Signaling Technologies, #9271), total AKT (Cell Signaling Technologies, #4685), phosphor p44/42 (ERK-1,2) (Thr202Tyr204) (Cell Signaling Technologies, #9101), total p44/42 ERK1/2 (Cell Signaling Technologies, #9102), total Grb2 (Cell Signaling Technologies, #3972), GSK-3β (Cell Signaling, D5C5Z), Vinculin (Sigma-Aldrich, MAB3574), secondary anti-rabbit IgG (GE Healthcare UK, NA934V), and secondary anti-mouse IgG (GE Healthcare UK, NA931V). Quantification of immunoblots was performed using ImageJ software.

Hyperinsulinemic-Euglycemic Clamps

At 5-6 days prior to the clamp, mice were anesthetized, and an indwelling catheter was placed in the right internal jugular vein. After recovery, mice were fasted overnight and placed in rat restrainers. After an acclimation period, a 2-hour hyperinsulinemic-euglycemic clamp was conducted in awake mice with a primed and continuous infusion of human insulin (150 mU/kg body-weight priming followed by 2.5mU/kg/min; Humulin, Eli Lilly & Co.) (59). To maintain euglycemia, 20% glucose was infused at variable rates during the clamp. Whole-body glucose turnover was assessed via a continuous infusion of [3-^{3}H]-glucose (PerkinElmer). To measure insulin-stimulated glucose uptake in individual organs, 2-deoxy-D-[1-^{14}C]-glucose was administered as a bolus (10 mCi) at 75 minutes after the start of the clamp. Whole body glycolysis was calculated from the rate of increase in plasma $^{3}H_2O$ concentrations from 80 to 120 minutes. Whole body glycogen plus lipid synthesis were estimated by subtracting whole body glycolysis from whole body glucose turnover. At the conclusion of the clamp, mice were anesthetized, and tissues were harvested, snap frozen in liquid nitrogen and kept at -80 C^{o} until analysis.

Statistical Analyses

Data are presented as mean ± SEM. Comparisons between two groups were analyzed using an unpaired two-tailed Student *t* test. Comparison between more than two groups was performed using one-way ANOVA or two-way ANOVA with repeated measures followed by post hoc t tests, as appropriate. Statistical analysis was performed using GraphPad Prism (Version 7.02). Significance level was set at *P < .05, **P < .01, *** P <.001, and ****P < .0001.

Study Approval

All animal protocols were approved by the Institutional Animal Care and Use Committee of the Joslin Diabetes Center and University of Massachusetts Medical School and were in accordance with National Institutes of Health guidelines.

Author Contributions

EPH designed the research studies, conducted the experiments, acquired, and analyzed the data, and wrote the manuscript. BBB, SS, AEL, BTO, RNK, and JKK assisted in the experimental design, acquiring and analyzing data and helped write the manuscript. CRK designed the study, supervised all work, and helped write the manuscript.

Acknowledgements

This work was supported by NIH Grants T32DK007260 (EPH), R01DK067536 (RNK) R01DK103215 (RNK), R01DK031036 (CRK), and R01DK082659 (CRK). The clamp study was conducted by the National Mouse Metabolic Phenotyping Center at UMass Medical School funded by an NIH grant (5U2C-DK093000 to J.K.K.). We thank Hye Lim Noh and Sujin Suk for their assistance with the clamp study. We thank Jennifer Hollister-Lock and Gordon Weir for their assistance with the *in vitro* glucose stimulate insulin secretion assays. We thank Jane Hu for her assistance with quantifying beta-cell mass and proliferation. We thank Domenico Accili for providing the *Foxo1*, *Foxo3*, and *Foxo4* floxed mice. We thank Mengyao Ella Li and Kristina M. Kriauciunas for their assistance with the insulin signaling analysis. We thank Masaji Sakaguchi and Christie Penniman for their help with conducting *in vivo* metabolic assays. We thank Allen Clermont and the Animal Physiology Core of the Joslin Diabetes Research Center, which is supported by (DRC) (P30 DK036836). We thank Dana-Farber/Harvard Cancer Center in Boston, MA, for the use of the Rodent Histopathology Core, which provided tissue embedding, sectioning, and H&E staining services. Dana-Farber/Harvard Cancer Center is supported in part by a NCI Cancer Center Support Grant # NIH 5 P30 CA06516. Graphical abstract was created with Biorender.

References

1. Boucher J, Tseng YH, and Kahn CR. Insulin and insulin-like growth factor-1 receptors act as ligand-specific amplitude modulators of a common pathway regulating gene transcription. *J Biol Chem.* 2010;285(22):17235-45.
2. Boucher J, Kleinridders A, and Kahn CR. Cold Spring Harbor Laboratory Press; 2013:409.
3. Ghaben AL, and Scherer PE. Adipogenesis and metabolic health. *Nat Rev Mol Cell Biol.* 2019;20(4):242-58.
4. Boucher J, Softic S, El Ouaamari A, Krumpoch MT, Kleinridders A, Kulkarni RN, et al. Differential Roles of Insulin and IGF-1 Receptors in Adipose Tissue Development and Function. *Diabetes.* 2016;65(8):2201-13.
5. Softic S, Boucher J, Solheim MH, Fujisaka S, Haering MF, Homan EP, et al. Lipodystrophy Due to Adipose Tissue-Specific Insulin Receptor Knockout Results in Progressive NAFLD. *Diabetes.* 2016;65(8):2187-200.
6. Sakaguchi M, Fujisaka S, Cai W, Winnay JN, Konishi M, O'Neill BT, et al. Adipocyte Dynamics and Reversible Metabolic Syndrome in Mice with an Inducible Adipocyte-Specific Deletion of the Insulin Receptor. *Cell Metab.* 2017;25(2):448-62.
7. Gross DN, van den Heuvel AP, and Birnbaum MJ. The role of FoxO in the regulation of metabolism. *Oncogene.* 2008;27(16):2320-36.
8. Tzivion G, Dobson M, and Ramakrishnan G. FoxO transcription factors; Regulation by AKT and 14-3-3 proteins. *Biochim Biophys Acta.* 2011;1813(11):1938-45.
9. Boucher J, Kleinridders A, and Kahn CR. Insulin receptor signaling in normal and insulin-resistant states. *Cold Spring Harb Perspect Biol.* 2014;6(1).
10. Kamagate A, Qu S, Perdomo G, Su D, Kim DH, Slusher S, et al. FoxO1 mediates insulin-dependent regulation of hepatic VLDL production in mice. *J Clin Invest.* 2008;118(6):2347-64.
11. Michael MD, Kulkarni RN, Postic C, Previs SF, Shulman GI, Magnuson MA, et al. Loss of insulin signaling in hepatocytes leads to severe insulin resistance and progressive hepatic dysfunction. *Mol Cell.* 2000;6(1):87-97.
12. O-Sullivan I, Zhang W, Wasserman DH, Liew CW, Liu J, Paik J, et al. FoxO1 integrates direct and indirect effects of insulin on hepatic glucose production and glucose utilization. *Nature communications.* 2015;6:7079-.
13. O'Neill BT, Lauritzen HP, Hirshman MF, Smyth G, Goodyear LJ, and Kahn CR. Differential Role of Insulin/IGF-1 Receptor Signaling in Muscle Growth and Glucose Homeostasis. *Cell reports.* 2015;11(8):1220-35.
14. O'Neill BT, Lee KY, Klaus K, Softic S, Krumpoch MT, Fentz J, et al. Insulin and IGF-1 receptors regulate FoxO-mediated signaling in muscle proteostasis. *J Clin Invest.* 2016;126(9):3433-46.
15. O'Neill BT, Bhardwaj G, Penniman CM, Krumpoch MT, Suarez Beltran PA, Klaus K, et al. FoxO Transcription Factors Are Critical Regulators of Diabetes-Related Muscle Atrophy. *Diabetes.* 2019;68(3):556-70.
16. El Ouaamari A, Dirice E, Gedeon N, Hu J, Zhou JY, Shirakawa J, et al. SerpinB1 Promotes Pancreatic beta Cell Proliferation. *Cell Metab.* 2016;23(1):194-205.

17. Barthel A, Schmoll D, and Unterman TG. FoxO proteins in insulin action and metabolism. *Trends Endocrinol Metab.* 2005;16(4):183-9.
18. Ogg S, Paradis S, Gottlieb S, Patterson GI, Lee L, Tissenbaum HA, et al. The Fork head transcription factor DAF-16 transduces insulin-like metabolic and longevity signals in C. elegans. *Nature.* 1997;389(6654):994-9.
19. Gesta S, Tseng YH, and Kahn CR. Developmental origin of fat: tracking obesity to its source. *Cell.* 2007;131(2):242-56.
20. Nakae J, Kitamura T, Kitamura Y, Biggs WH, 3rd, Arden KC, and Accili D. The forkhead transcription factor Foxo1 regulates adipocyte differentiation. *Dev Cell.* 2003;4(1):119-29.
21. van der Vos KE, and Coffer PJ. FOXO-binding partners: it takes two to tango. *Oncogene.* 2008;27(16):2289-99.
22. Tsuchiya K, and Ogawa Y. Forkhead box class O family member proteins: The biology and pathophysiological roles in diabetes. *J Diabetes Investig.* 2017;8(6):726-34.
23. Fan W, Imamura T, Sonoda N, Sears DD, Patsouris D, Kim JJ, et al. FOXO1 transrepresses peroxisome proliferator-activated receptor gamma transactivation, coordinating an insulin-induced feed-forward response in adipocytes. *J Biol Chem.* 2009;284(18):12188-97.
24. Chakrabarti P, and Kandror KV. FoxO1 controls insulin-dependent adipose triglyceride lipase (ATGL) expression and lipolysis in adipocytes. *J Biol Chem.* 2009;284(20):13296-300.
25. Kahn CR, Wang G, and Lee KY. Altered adipose tissue and adipocyte function in the pathogenesis of metabolic syndrome. *J Clin Invest.* 2019;129(10):3990-4000.
26. Lee KY, Luong Q, Sharma R, Dreyfuss JM, Ussar S, and Kahn CR. Developmental and functional heterogeneity of white adipocytes within a single fat depot. *EMBO J.* 2019;38(3).
27. Ramirez AK, Dankel SN, Rastegarpanah B, Cai W, Xue R, Crovella M, et al. Single-cell transcriptional networks in differentiating preadipocytes suggest drivers associated with tissue heterogeneity. *Nat Commun.* 2020;11(1):2117.
28. Min SY, Desai A, Yang Z, Sharma A, DeSouza T, Genga RMJ, et al. Diverse repertoire of human adipocyte subtypes develops from transcriptionally distinct mesenchymal progenitor cells. *Proc Natl Acad Sci U S A.* 2019;116(36):17970-9.
29. Wajchenberg BL. Subcutaneous and visceral adipose tissue: their relation to the metabolic syndrome. *Endocr Rev.* 2000;21(6):697-738.
30. Davis KE, M DN, Sun K, W MS, J DB, J AZ, et al. The sexually dimorphic role of adipose and adipocyte estrogen receptors in modulating adipose tissue expansion, inflammation, and fibrosis. *Mol Metab.* 2013;2(3):227-42.
31. Schoettl T, Fischer IP, and Ussar S. Heterogeneity of adipose tissue in development and metabolic function. *The Journal of experimental biology.* 2018;221(Pt Suppl 1).
32. Tseng YH, Kokkotou E, Schulz TJ, Huang TL, Winnay JN, Taniguchi CM, et al. New role of bone morphogenetic protein 7 in brown adipogenesis and energy expenditure. *Nature.* 2008;454(7207):1000-4.
33. Schulz TJ, and Tseng YH. Emerging role of bone morphogenetic proteins in adipogenesis and energy metabolism. *Cytokine Growth Factor Rev.* 2009;20(5-6):523-31.

34. Kadowaki T, Yamauchi T, Kubota N, Hara K, Ueki K, and Tobe K. Adiponectin and adiponectin receptors in insulin resistance, diabetes, and the metabolic syndrome. *J Clin Invest.* 2006;116(7):1784-92.
35. Stanford KI, Middelbeek RJ, Townsend KL, Lee MY, Takahashi H, So K, et al. A novel role for subcutaneous adipose tissue in exercise-induced improvements in glucose homeostasis. *Diabetes.* 2015;64(6):2002-14.
36. Stanford KI, Middelbeek RJ, Townsend KL, An D, Nygaard EB, Hitchcox KM, et al. Brown adipose tissue regulates glucose homeostasis and insulin sensitivity. *J Clin Invest.* 2013;123(1):215-23.
37. Bluher M. Neuregulin 4: A "Hotline" Between Brown Fat and Liver. *Obesity (Silver Spring).* 2019;27(10):1555-7.
38. Thomou T, Mori MA, Dreyfuss JM, Konishi M, Sakaguchi M, Wolfrum C, et al. Adipose-derived circulating miRNAs regulate gene expression in other tissues. *Nature.* 2017;542(7642):450-5.
39. Berg AH, Combs TP, Du X, Brownlee M, and Scherer PE. The adipocyte-secreted protein Acrp30 enhances hepatic insulin action. *Nat Med.* 2001;7(8):947-53.
40. Stern JH, Rutkowski JM, and Scherer PE. Adiponectin, Leptin, and Fatty Acids in the Maintenance of Metabolic Homeostasis through Adipose Tissue Crosstalk. *Cell Metab.* 2016;23(5):770-84.
41. Wang GX, Zhao XY, and Lin JD. The brown fat secretome: metabolic functions beyond thermogenesis. *Trends Endocrinol Metab.* 2015;26(5):231-7.
42. Kruszynska YT, Worrall DS, Ofrecio J, Frias JP, Macaraeg G, and Olefsky JM. Fatty acid-induced insulin resistance: decreased muscle PI3K activation but unchanged Akt phosphorylation. *J Clin Endocrinol Metab.* 2002;87(1):226-34.
43. Liu XJ, He AB, Chang YS, and Fang FD. Atypical protein kinase C in glucose metabolism. *Cell Signal.* 2006;18(12):2071-6.
44. Standaert ML, Kanoh Y, Sajan MP, Bandyopadhyay G, and Farese RV. Cbl, IRS-1, and IRS-2 mediate effects of rosiglitazone on PI3K, PKC-lambda, and glucose transport in 3T3/L1 adipocytes. *Endocrinology.* 2002;143(5):1705-16.
45. Petersen MC, Vatner DF, and Shulman GI. Regulation of hepatic glucose metabolism in health and disease. *Nat Rev Endocrinol.* 2017;13(10):572-87.
46. Scherer T, O'Hare J, Diggs-Andrews K, Schweiger M, Cheng B, Lindtner C, et al. Brain insulin controls adipose tissue lipolysis and lipogenesis. *Cell Metab.* 2011;13(2):183-94.
47. Sechi LA, Melis A, and Tedde R. Insulin hypersecretion: a distinctive feature between essential and secondary hypertension. *Metabolism.* 1992;41(11):1261-6.
48. Najjar SM, and Perdomo G. Hepatic Insulin Clearance: Mechanism and Physiology. *Physiology (Bethesda).* 2019;34(3):198-215.
49. Robertson RP, Harmon J, Tran PO, and Poitout V. Beta-cell glucose toxicity, lipotoxicity, and chronic oxidative stress in type 2 diabetes. *Diabetes.* 2004;53 Suppl 1:S119-24.
50. El Ouaamari A, Kawamori D, Dirice E, Liew CW, Shadrach JL, Hu J, et al. Liver-derived systemic factors drive beta cell hyperplasia in insulin-resistant states. *Cell reports.* 2013;3(2):401-10.

51. Bruning JC, Michael MD, Winnay JN, Hayashi T, Horsch D, Accili D, et al. A muscle-specific insulin receptor knockout exhibits features of the metabolic syndrome of NIDDM without altering glucose tolerance. *Mol Cell.* 1998;2(5):559-69.
52. Holzenberger M, Leneuve P, Hamard G, Ducos B, Perin L, Binoux M, et al. A targeted partial invalidation of the insulin-like growth factor I receptor gene in mice causes a postnatal growth deficit. *Endocrinology.* 2000;141(7):2557-66.
53. Paik JH, Kollipara R, Chu G, Ji H, Xiao Y, Ding Z, et al. FoxOs are lineage-restricted redundant tumor suppressors and regulate endothelial cell homeostasis. *Cell.* 2007;128(2):309-23.
54. Castrillon DH, Miao L, Kollipara R, Horner JW, and DePinho RA. Suppression of ovarian follicle activation in mice by the transcription factor Foxo3a. *Science.* 2003;301(5630):215-8.
55. Pagliuca FW, Millman JR, Gurtler M, Segel M, Van Dervort A, Ryu JH, et al. Generation of functional human pancreatic beta cells in vitro. *Cell.* 2014;159(2):428-39.
56. Debosch BJ, Chen Z, Saben JL, Finck BN, and Moley KH. Glucose transporter 8 (GLUT8) mediates fructose-induced de novo lipogenesis and macrosteatosis. *J Biol Chem.* 2014;289(16):10989-98.
57. Boucher J, Mori MA, Lee KY, Smyth G, Liew CW, Macotela Y, et al. Impaired thermogenesis and adipose tissue development in mice with fat-specific disruption of insulin and IGF-1 signalling. *Nat Commun.* 2012;3:902.
58. Lee KY, Gesta S, Boucher J, Wang XL, and Kahn CR. The differential role of Hif1beta/Arnt and the hypoxic response in adipose function, fibrosis, and inflammation. *Cell Metab.* 2011;14(4):491-503.
59. Kim JK. Hyperinsulinemic-euglycemic clamp to assess insulin sensitivity in vivo. *Methods Mol Biol.* 2009;560:221-38.

Figures and Figure Legends

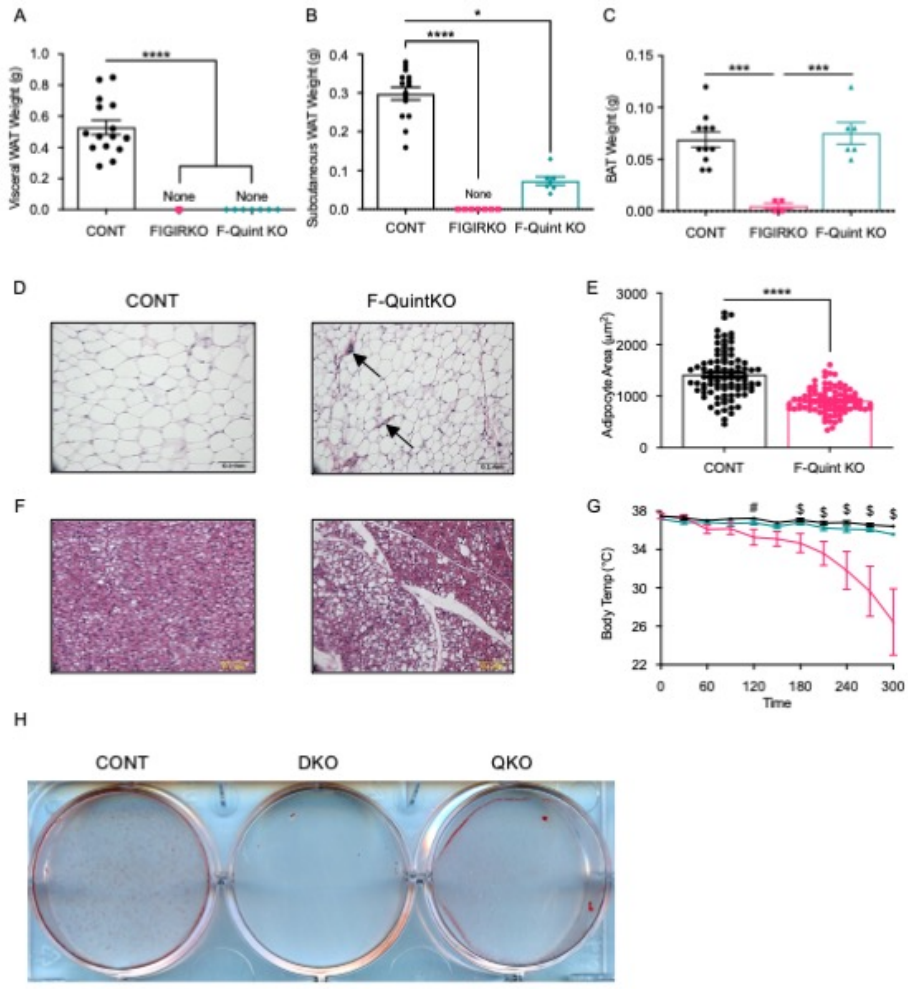

Figure 1. Partial recovery of subcutaneous WAT and recovery of functional brown adipose tissue with fat specific deletion of *Foxo1/3/4* in F-Quint KO mice. A-C) Ad lib fed CONT, FIGIRKO and F-Quint KO mice were sacrificed at 3 months of age and visceral (perigonadal) WAT (A), subcutaneous (inguinal) WAT (B), and BAT (C) were removed and weighed. Results represent 4-11 mice per group. Statistics were performed using a one-way ANOVA, where **P* < .05, *** P <.001, and *****P* < .0001. D) H&E-stained sections of subcutaneous tissues from the same mice in panel B. Scale bar: 0.1mm. Arrows indicate areas of lymphocyte infiltration. E) Average adipocyte area was measured subcutaneous tissues from same mice in panel B. Statistics were performed using a two-way ANOVA, where *****P* < .0001. F) H&E-stained sections of BAT tissues from the same mice in panel C. Scale bar: 0.1mm. G) Rectal temperature was measured in 3-month-old mice every 30 minutes for 3h during exposure to a 6^{o}C environment. Results represent 4-11 mice per group. Statistics were performed using a two-way ANOVA with repeated measures, where # represents p<0.05 CONT vs FIGIRKO, and $ represents p<0.05 CONT vs FIGIRKO and FIGIRKO vs. F-Quint KO. H) Images of subcutaneous-derived CONT, DKO, and QKO adipocyte cell lines stained with Oil Red O after *in vitro* adipogenic differentiation. Each image is one representative well of 6-well plate.

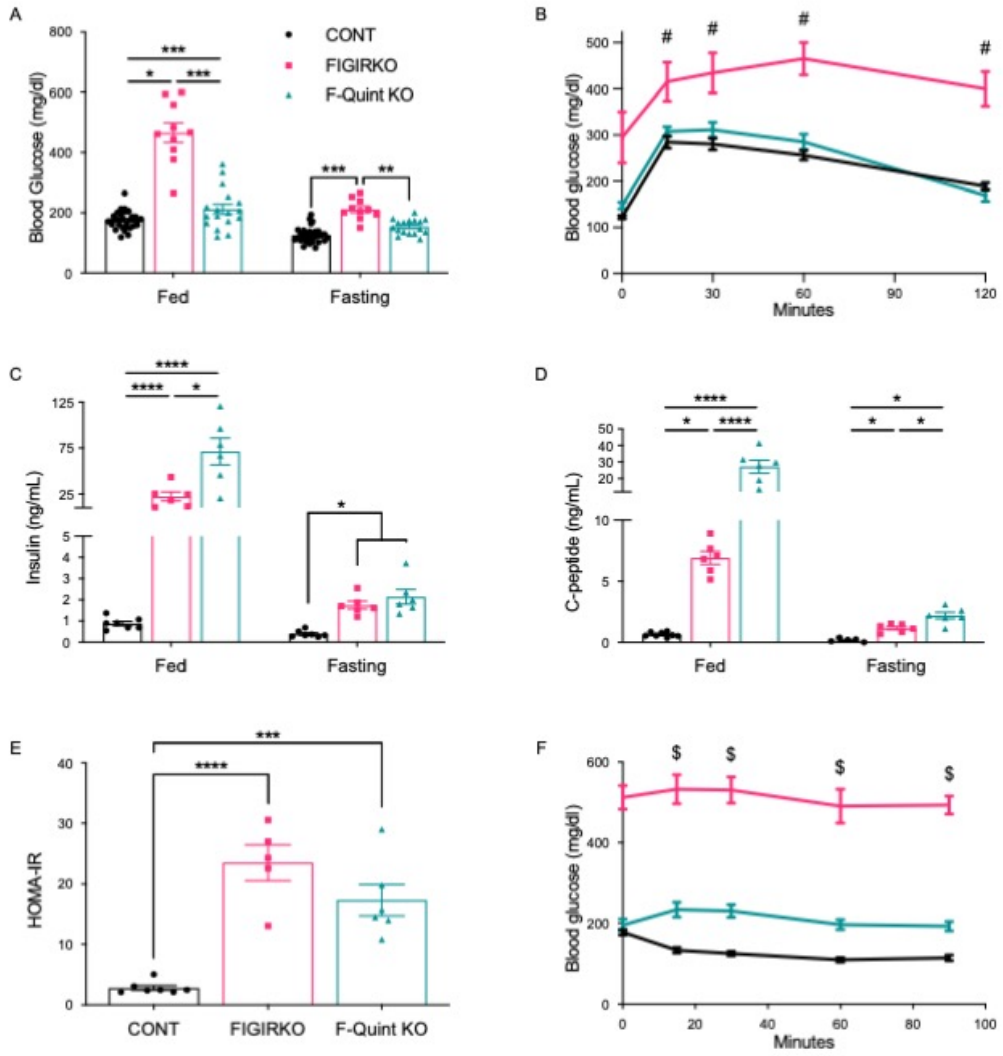

Figure 2. Recovery of glucose homeostasis and worsening of hyperinsulinemia in F-Quint KO mice. A) Blood glucose in 12-week-old, fed and fasting mice. Results represent 10-32 mice per group. Statistics were performed using a one-way ANOVA, where *P < .05, **P < .01, and *** P <.001. B) Glucose tolerance tests of control, FIGIRKO, and F-Quint KO mice at 12-weeks of age. Results represent 5-15 mice per group. Statistics were performed using a two-way ANOVA with repeated measures, where # represents p<0.05 between CONT vs FIGIRKO and FIGIRKO vs F-Quint KO. C-D) Serum insulin (C) and C-peptide (D) levels in the fed or fasted state in 12-week old control, FIGIRKO, and F-Quint KO mice. Results represent 6-8 mice per group. Statistics were performed using a one-way ANOVA; where *P < .05, and ****P < .0001. E) HOMA-IR was calculated for CONT, FIGIRKO, and F-Quint KO mice at 12-weeks old. Results represent 5-7 mice per group is shown. Statistics were performed using a one-way ANOVA; where *** P <.001, and ****P < .0001.. F) Insulin tolerance test of CONT, FIGIRKO, and F-Quint KO mice at 12-weeks of age. Results represent 5-22 mice per group. Statistics were performed using a two-way ANOVA with repeated measures, where $ represents p<0.05 between CONT vs FIGIRKO, CONT vs. F-Quint KO, and FIGIRKO vs F-Quint KO.

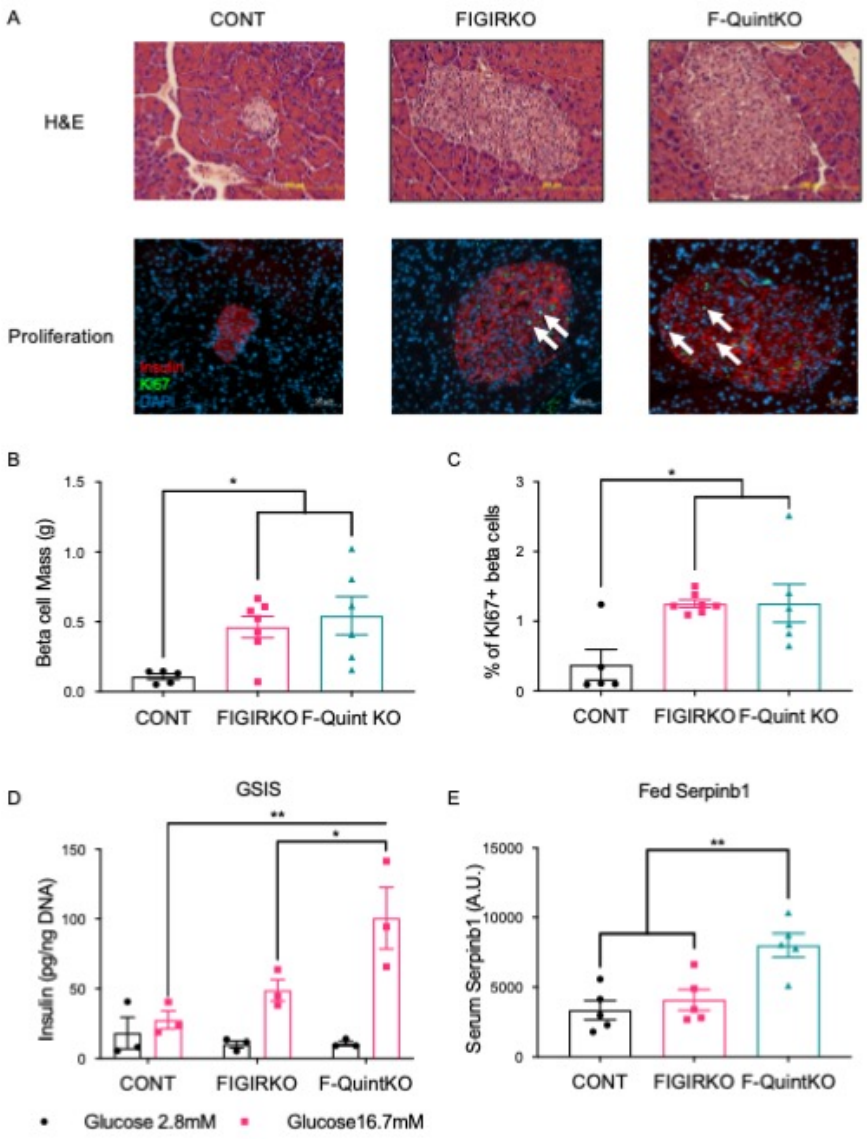

Figure 3- β-Cell hyperplasia remains despite loss of *FOXO1/3/4* in F-Quint KO mice. A) H&E and immunofluorescence staining for insulin, Ki67, and DAPI in pancreatic sections of CONT, FIGIRKO, and F-Quint KO mice at 12-weeks of age. Scale bar: 200μm for H&E staining and 50μm for immunofluorescence. White arrows indicate Ki67+ β-cells. B) Beta cell mass relative to total pancreas mass and C) the percent of Ki67+ beta cells were measured. Results represent 5-7 mice per group. Statistics were performed using a one-way ANOVA, where * represents $p<0.05$. D) *In vitro* GSIS results represent 3 per group. Statistics were performed using a two-way ANOVA, where $*P < .05$, and $**P < .01$. E) Densitometric quantification of SERPINB1 serum protein levels in the fed state determined by western blot analysis in 12-week-old mice. Results represent 4-5 mice per group. Statistics were performed using a one-way ANOVA, where $**P < .01$.

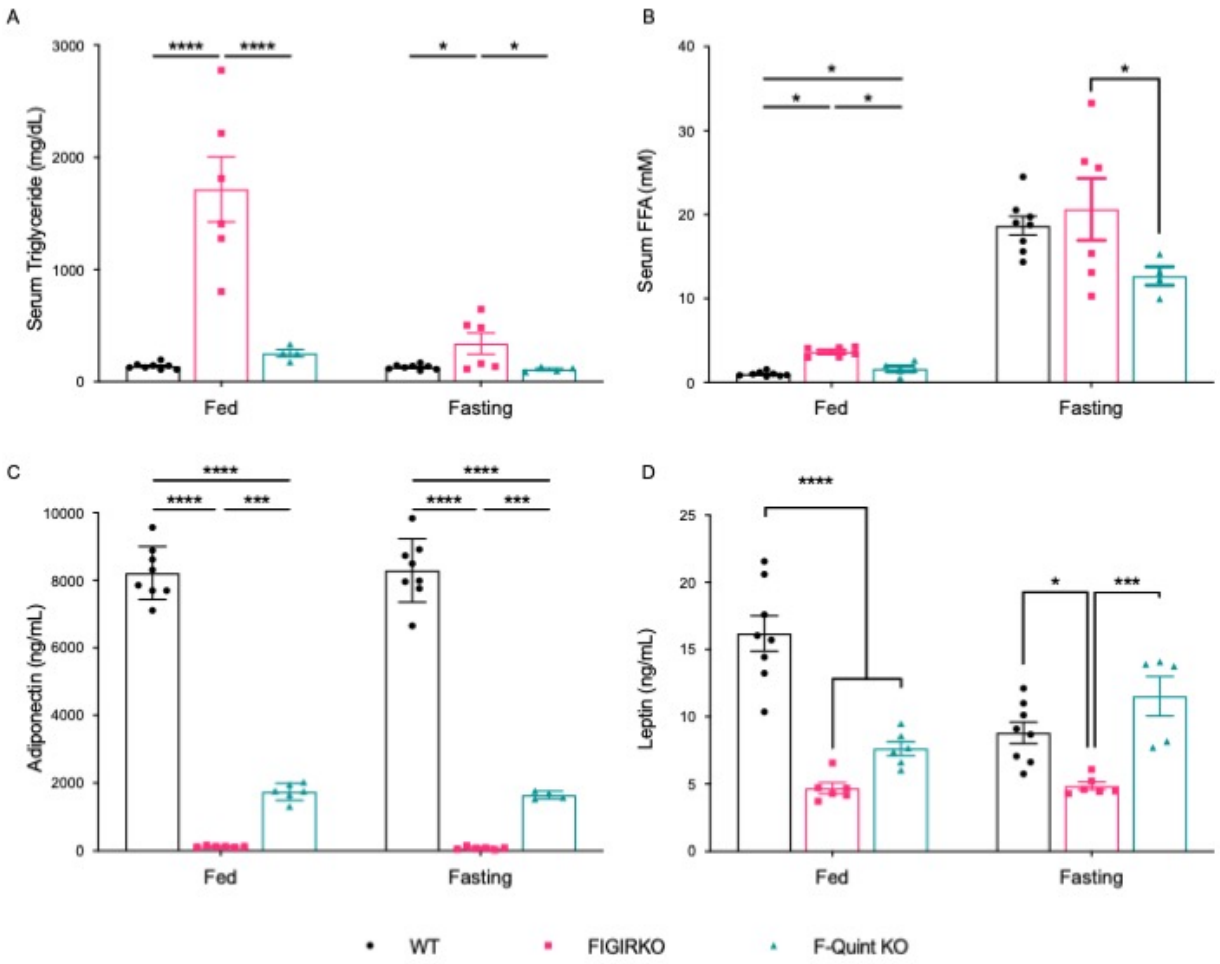

Figure 4. Partial recovery of serum triglyceride, free fatty acid, and adipokine levels in F-Quint KO mice. A-D) Serum triglyceride (A), free fatty acids (B), adiponectin (C), and leptin (D) were measured as described in Methods in fed and fasting mice at 3-months of age. Results represent 6-8 mice per group. Statistics were performed using a one-way ANOVA; where *P < .05, *** P <.001, and ****P < .0001

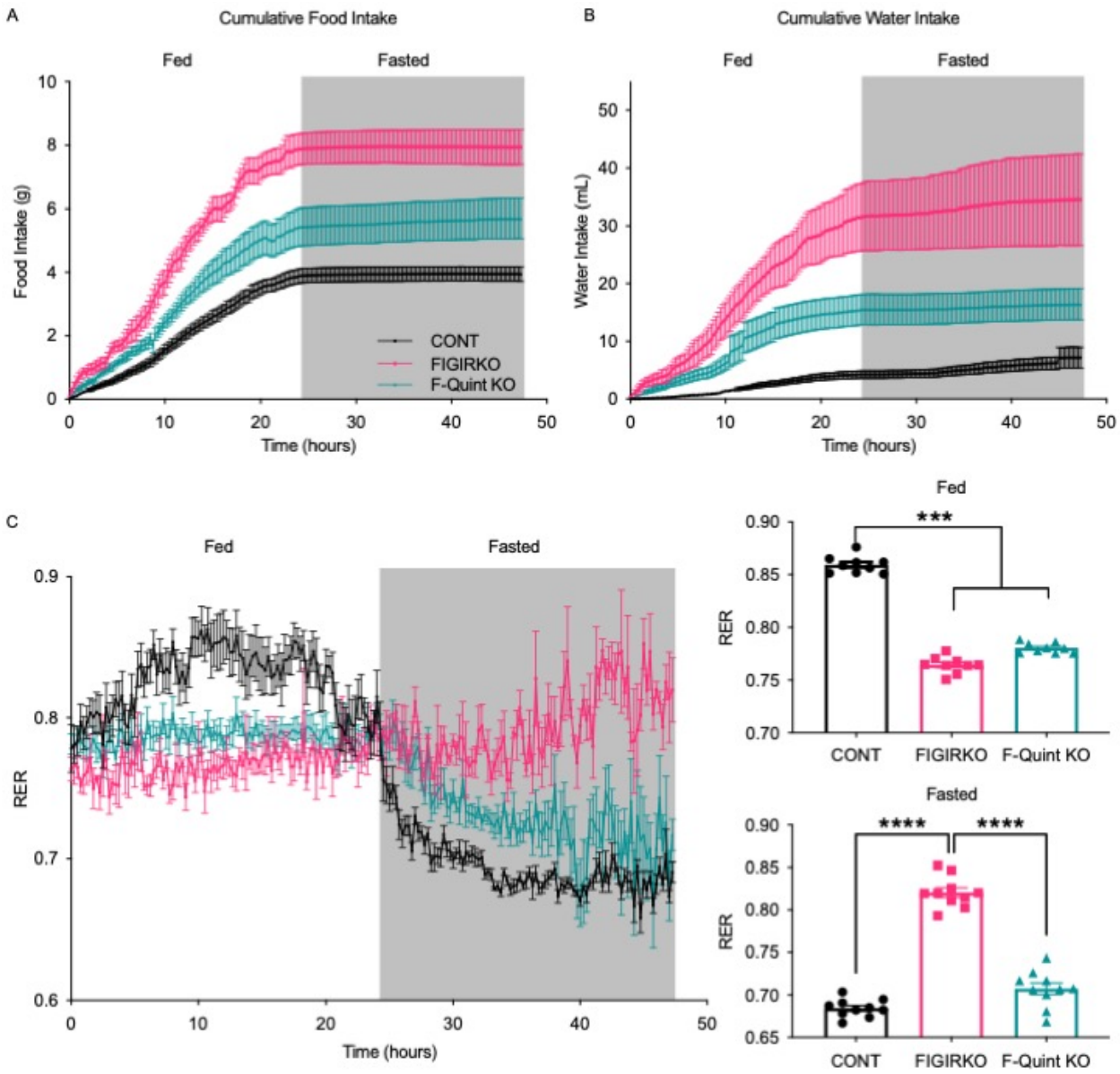

Figure 5. Improvement in food intake and water intake and fasted energy expenditure with loss of *FOXO1/3/4* in F-Quint KO mice. A-C) Food intake (A), water intake (B) and RER (C) of 12-week-old CONT, FIGIRKO, and F-Quint KO mice were measured using CLAMS metabolic cages. Results represent 3-10 mice per group. Statistics were performed using a one-way ANOVA; where ***P < .001, ****P < .0001.

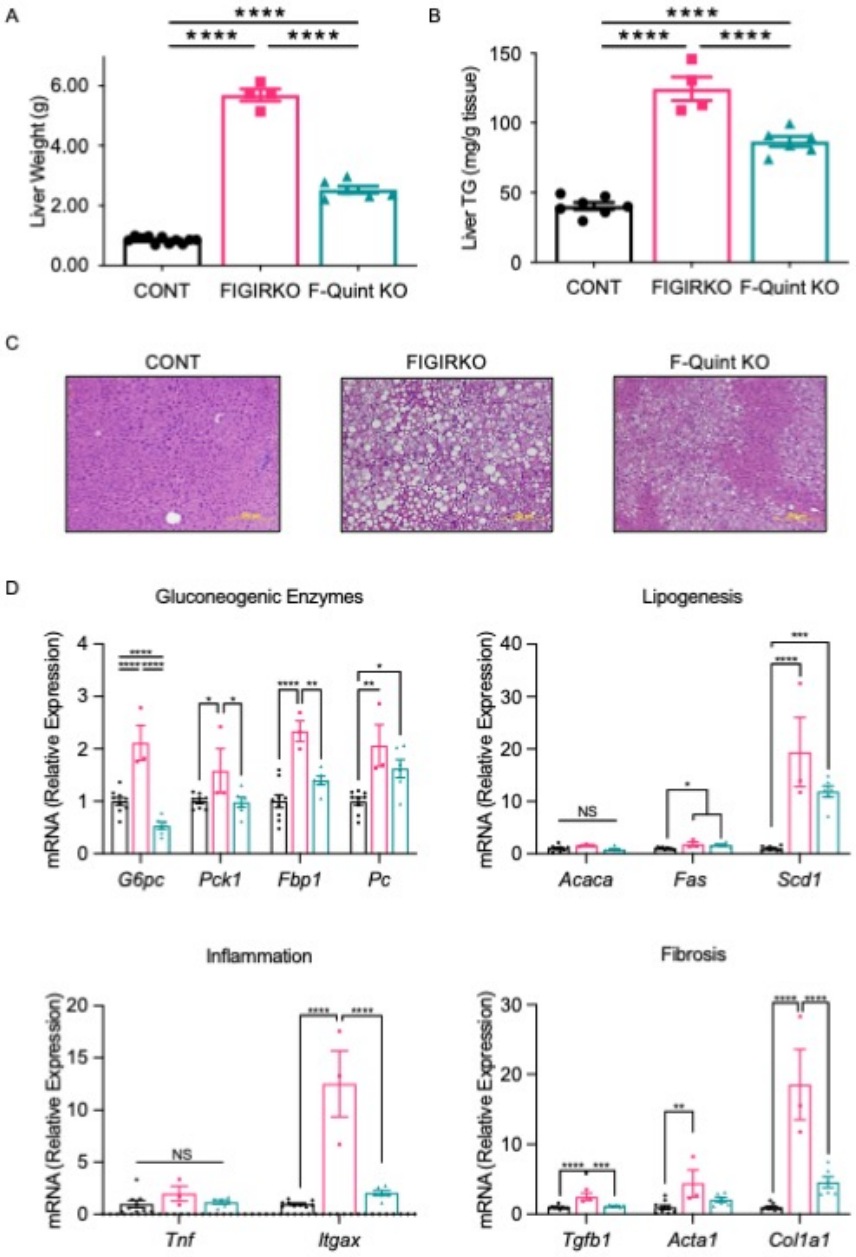

Figure 6. Partial rescue of hepatosteatosis in F-Quint KO mice. A-B) Liver weight (A) and liver TG content (mg/g tissue) (B) in CONT, FIGIRKO, and F-Quint KO mice at 3-months of age. Results represent 4-7 mice per group. Statistics were performed using ay one-way ANOVA, where ****P < .0001. C) H&E stained liver sections from CONT, FIGIRKO, and F-Quint KO mice at 3-months of age. Scale bar: 100μm. D) mRNA expression of genes involved in gluconeogenic enzymes, de novo lipogenesis, inflammation, and fibrosis in the livers of chow-fed CONT, FIGIRKO, and F-Quint KO mice at 3-months of age. Results represent 3-10 mice per group. Statistics were performed using a one-way ANOVA; *P < .05, **P < .01, *** P <.001, and ****P < .0001.

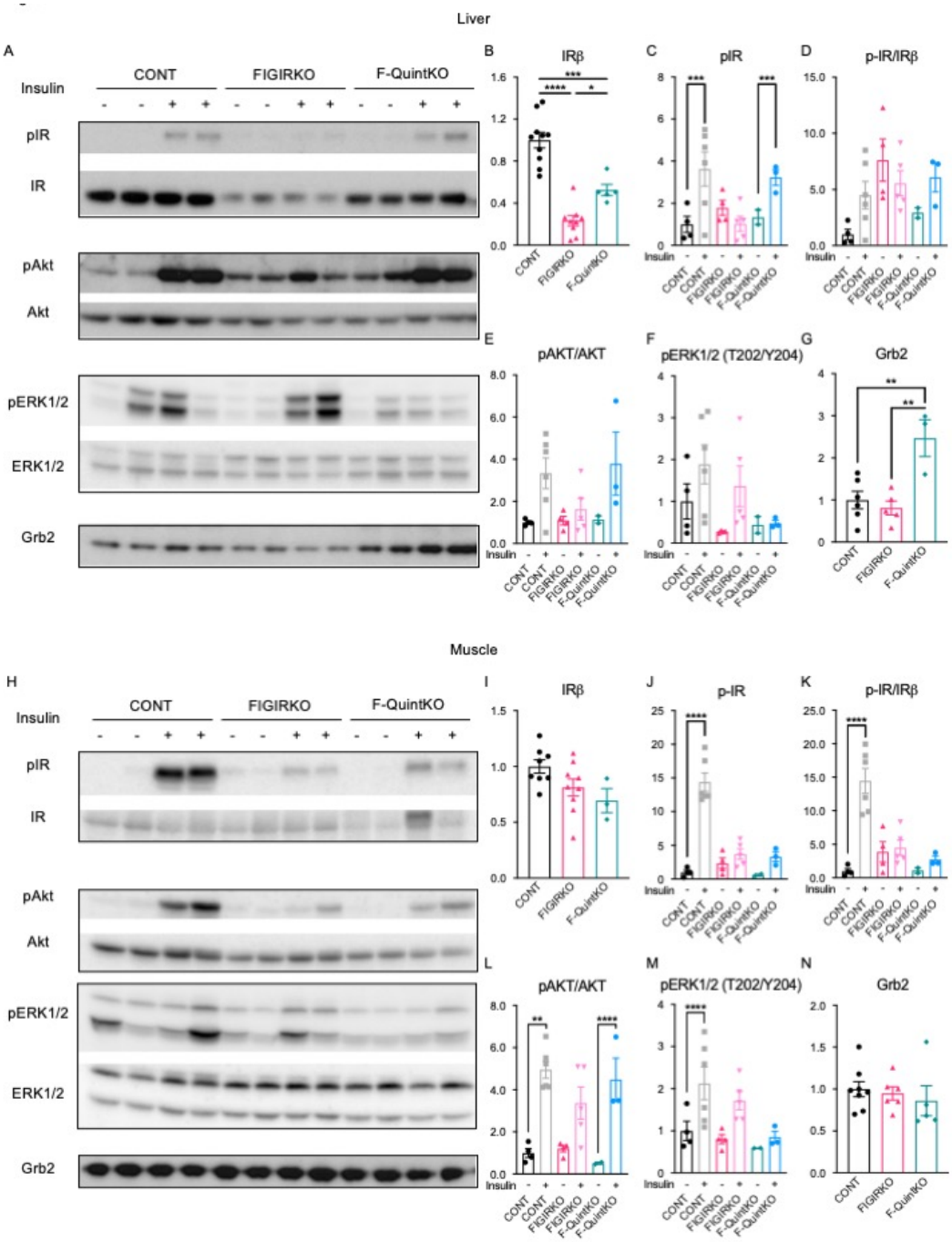

Figure 7. Restoration of liver insulin sensitivity in the context of whole-body insulin resistance in F-Quint KO mice. A-G) Western blot (A) and densitometric quantification of phosphorylated IR (pIR) (B), total IR-beta (C), pIR/IRbeta (D), pAKT/AKT (E), pERK1/2 (F), and Grb2 (G) in liver of 3-month-old mice. H-N) Western blot (H) and densitometric quantification of protein levels of phosphorylated IR (pIR) (I), total IR-beta (J), pIR/IRbeta (K), pAKT/AKT (L), pERK1/2 (M), and Grb2 (N) in soleus muscle of 3-month-old mice. Results represent 3-4 mice per group. Statistics were performed using a one-way ANOVA, where *P < .05, **P < .01, *** P <.001, and ****P < .0001.

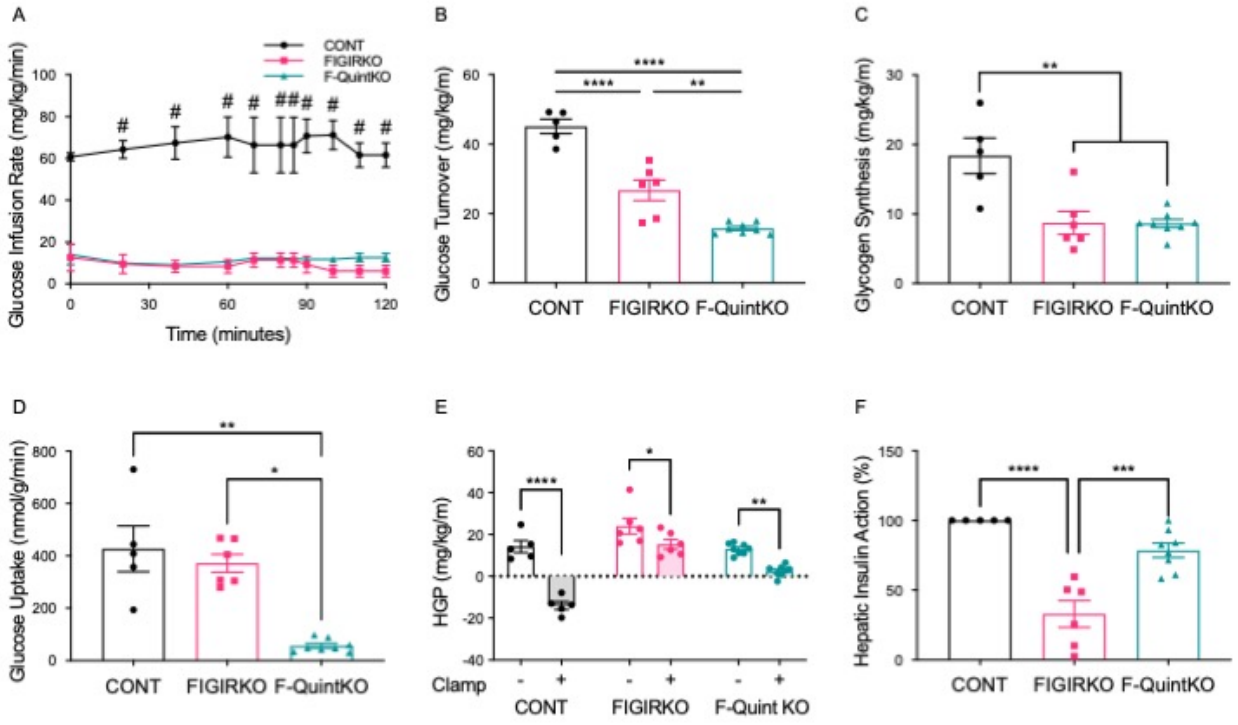

Figure 8. Restoration of liver insulin sensitivity in the context of whole-body insulin resistance in F-Quint KO mice. A) Glucose infusion rate adjusted every 10-20 minutes over the course of a hyperinsulinemic-euglycemic clamp in 3-month CONT, FIGIRKO, F-Quint KO mice. Results represent 5-8 mice per group. Statistics were performed using a two-way ANOVA with repeated measures, where # represents $p<0.05$ between CONT vs FIGIRKO and CONT vs F-Quint KO. B-F) Whole body glucose turnover (B), whole body glycogen plus lipid synthesis (C), insulin-stimulated glucose uptake in skeletal muscle (gastrocnemius) (D), basal and clamp HGP (E), and hepatic insulin action (F) measured during a hyperinsulinemic-euglycemic clamp in 3-month old CONT, FIGIRKO, and F-Quint KO mice. Results represent 5-8 mice per group. Statistics were performed using a one-way ANOVA; where *P < .05, **P < .01, *** P <.001, and ****P < .0001.

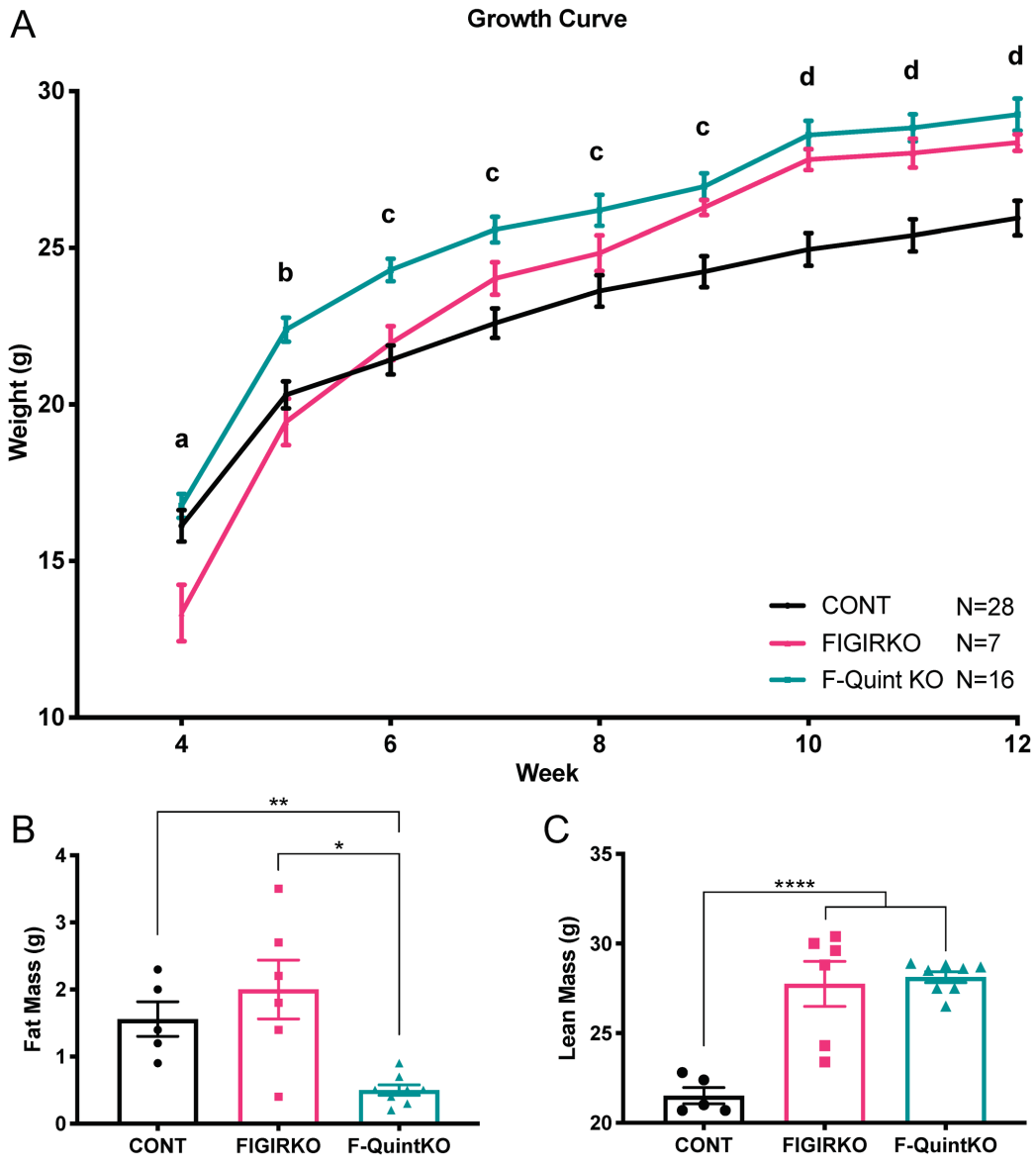

Supplemental Figure 1. F-Quint KO mice are normal at weaning but weight more than CONT by 12-weeks of age. A) Weight of CONT, FIGIRKO, and F-Quint KO mice were measured weekly from weaning (week 4) until 12 weeks of age. Results represent 7-28 mice per group. Statistics were performed using a two-way ANOVA with repeated measures, where a represents $p<0.05$ between FIGIRKO and CONT or F-Quint KO, b represents $p<0.05$ between FIGIRKO and F-Quint KO, c represents $p<0.05$ between CONT and F-Quint KO, and d represents $p<0.05$ between CONT and FIGIRKO or F-Quint KO. B-C) DEXA analysis assessed total body fat (B) and lean mass (C) in 12-week-old CONT, FIGIRKO, and F-Quint KO mice. Results represent 3-10 mice per group. Statistics were performed using a one-way ANOVA, where $*P < .05$, $**P < .01$, $****P < .0001$

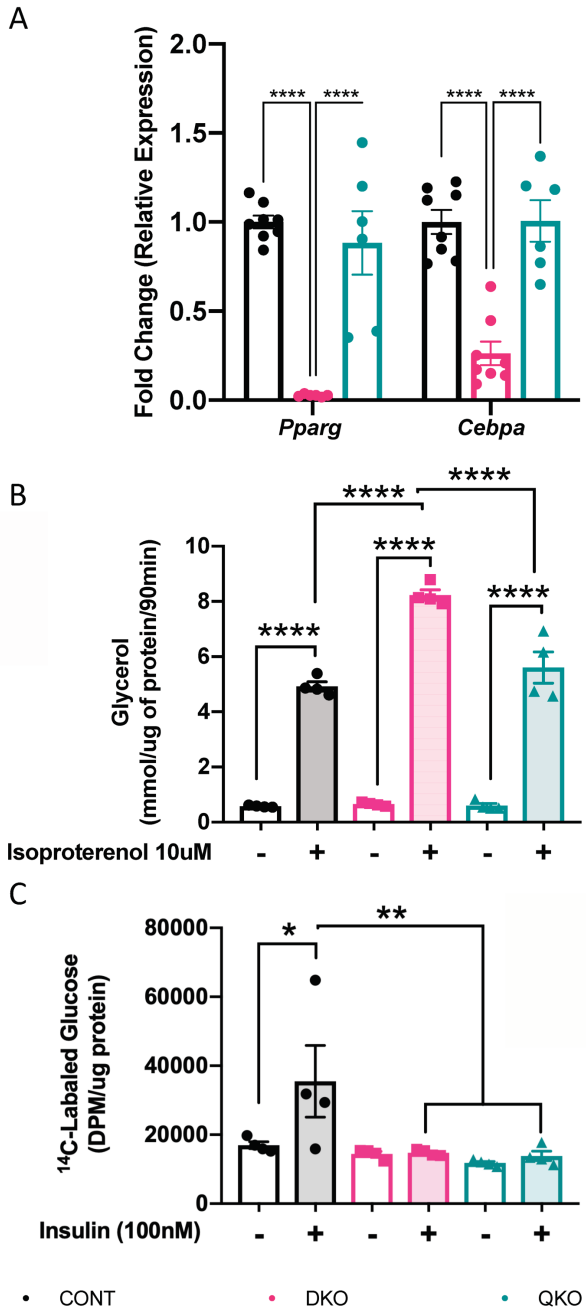

Supplemental Figure 2. Restoration of adipocyte differentiation and function with loss of FOXO1/3/4 in QKO cells. A) mRNA expression of the late adipogenic transcription factors, *Pparg* and *Cebpa,* in CONT, DKO, and QKO preadipocyte cells after differentiation for 4 days. Results represent 6-8 replicates per group. B) Lipolysis rates after stimulation with 10μM isoproterenol were measured by glycerol release from adipocytes after 9 days of adipogenic differentiation. Data are shown as mean ± SEM of 4 replicates and are normalized by lipid content of the cells. C) ^{14}C-Deoxy-D-glucose uptake in preadipocyte cell lines in the basal state and after pretreatment for 30 min with 100nM insulin. Uptake was measured for 10 minutes and data are shown as mean ± SEM of 4 samples. Statistics were performed using a one-way ANOVA, where *P < .05, **P < .01, ****P < .0001

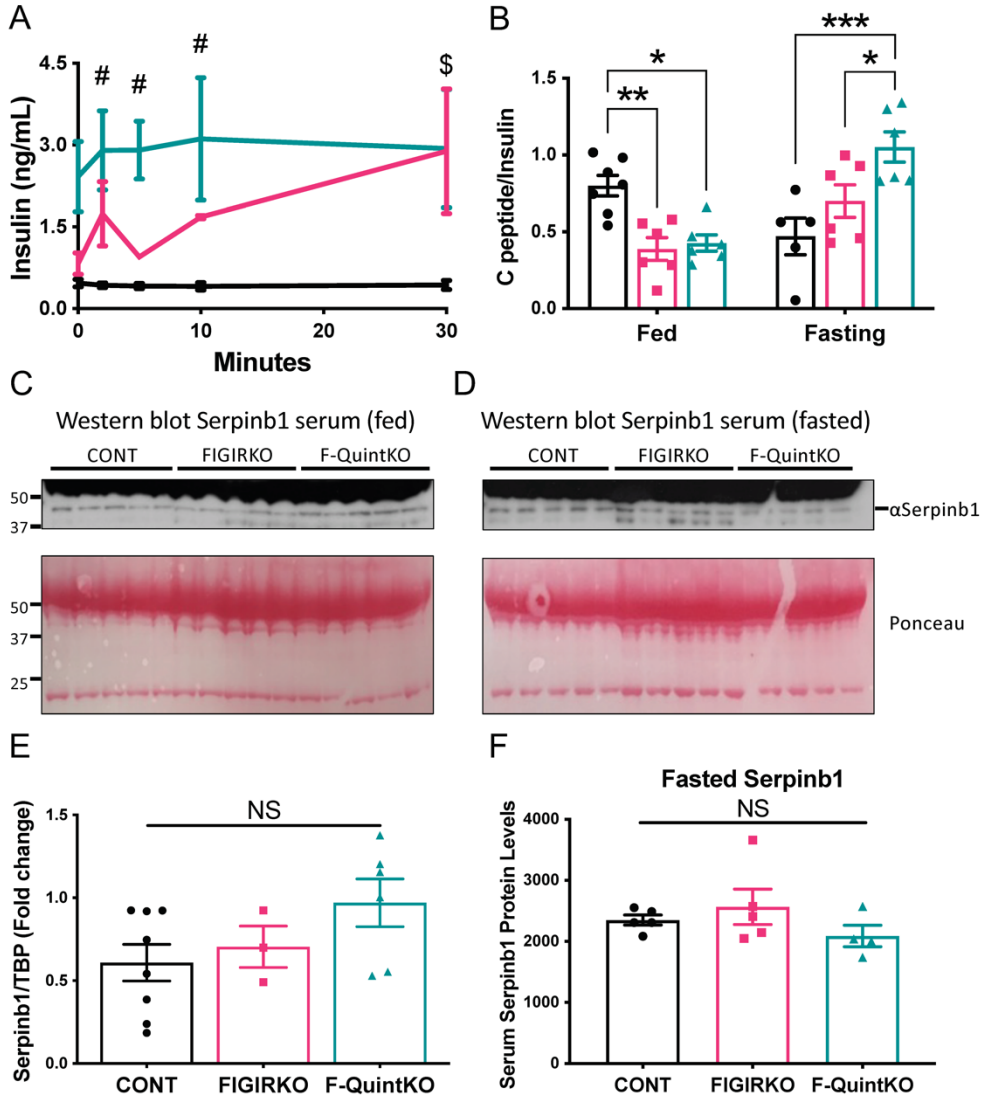

Supplemental Figure 3. β-Cell hyperplasia remains despite loss of FOXO1/3/4 in F-Quint KO mice. A) *In vivo* GSIS in CONT, FIGIRKO, and F-Quint KO mice at 3-months of age. Results represent 3-10 mice per group. Statistics were performed using a two-way ANOVA with repeated measures, where # represents p<0.05 CONT vs F-Quint KO, and $ represents p<0.05 CONT vs FIGIRKO and CONT vs. F-Quint KO. B) Insulin clearance measured by the ratio of C-peptide to insulin was calculated in 3-month-old CONT, FIGIRKO, and F-Quint KO mice in the fed and fasting state. Results represent 6-8 mice per group. Statistics were performed using a one-way ANOVA, where **P* < .05, ***P* < .01, and *** P <.001. C-D) Western blot of SERPINB1 in fed (C) and fasted (D) serum isolated from 3-month-old CONT, FIGIRKO, and F-Quint KO mice. Line indicates SERPINB1 band. E) mRNA expression of *Serpinb1* relative to *TBP* in liver of 3-month-old random fed CONT, FIGIRKO, F-Quint KO mice. Results represent 4-9 mice per group. Statistics were performed using a one-way ANOVA, where NS represents p>0.05. F) Densitometric quantification of SERPINB1 proteins levels relative to ponceau staining in serum of fasting 3-month-old CONT, FIGIRKO, and F-Quint KO mice. Results represent 4-5 mice per group. Statistics were performed using a one-way ANOVA, where NS represents p>0.05.

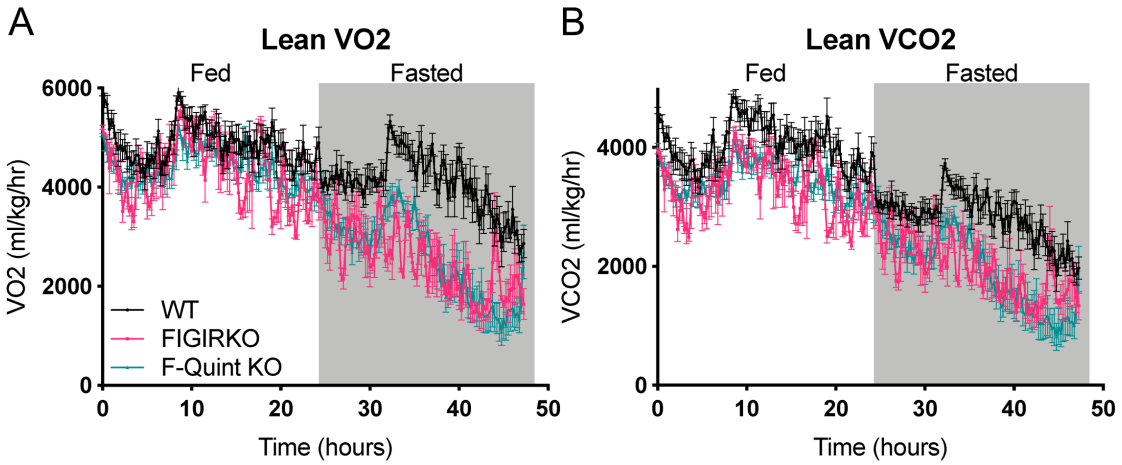

Supplemental Figure 4. Improvement in fasted energy expenditure with loss of FOXO1/3/4 in F-Quint KO mice. A-B) O2 utilization (A) and CO2 production (B) of 12-week-old CONT, FIGIRKO, and F-Quint KO mice were measured using metabolic cages and normalized to lean body mass. Results represent 3-10 mice per group.

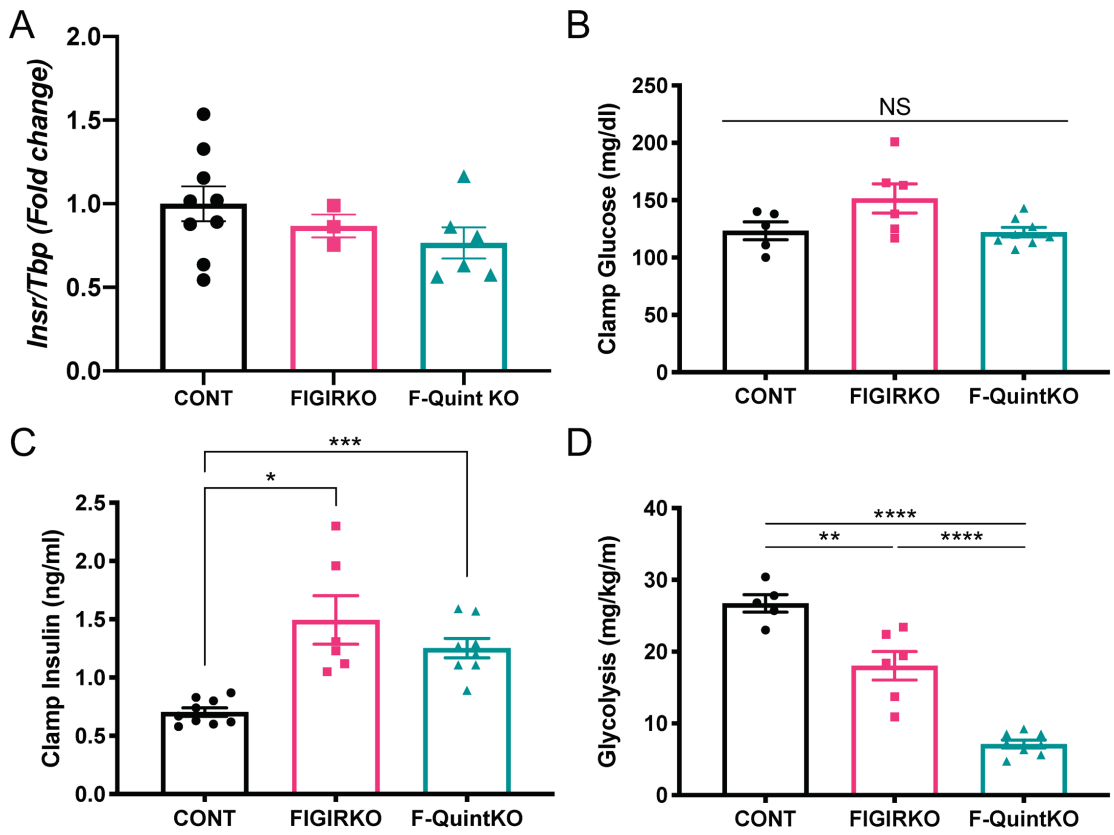

Supplemental Figure 5. Restoration of liver insulin sensitivity in the context of whole-body insulin resistance in F-Quint KO mice. mRNA expression of *Insr* in the livers of chow-fed CONT, FIGIRKO, and F-Quint KO mice at 3-months of age. Results represent 3-10 mice per group. Plasma glucose levels (B), Plasma insulin levels (C), and clamp HGP (D) were measured during a hyperinsulinemic-euglycemic clamp in 3-month old CONT, FIGIRKO, and F-Quint KO mice. Results represent 5-8 mice per group. Statistics were performed using a one-way ANOVA, where *P < .05, **P < .01, *** P <.001, and ****P < .0001.

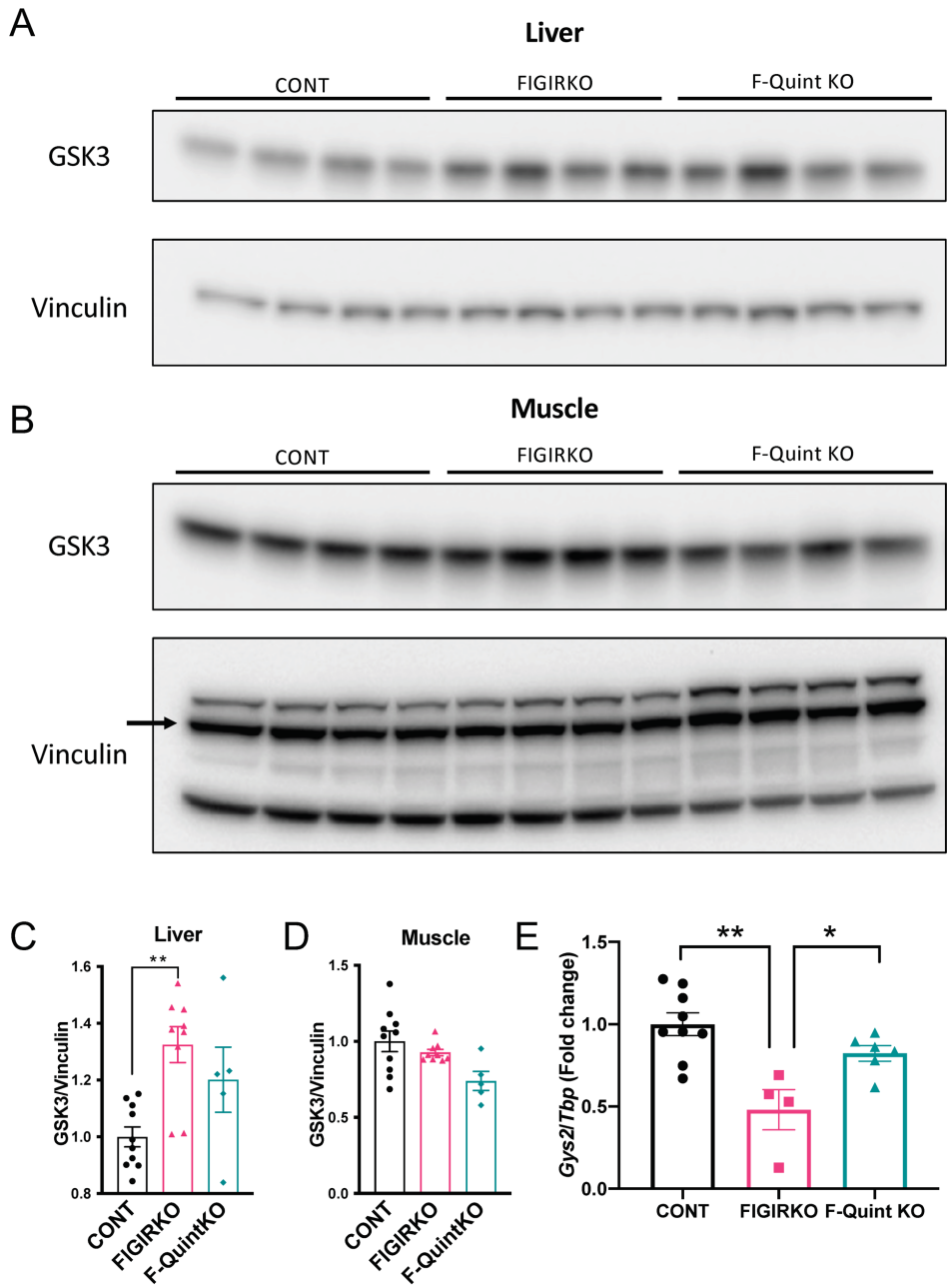

Supplemental Figure 6. Partial restoration of liver GSK3 levels and *Gys2* expression in F-Quint KO mice. A-B) Western blot of GSK3 relative to Vinculin in liver (A) and muscle (B) isolated from 3-month-old CONT, FIGIRKO, and F-Quint KO mice. Line indicates Vinculin band. C-D) Densitometric quantification of GSK3 proteins levels relative to Vinculin in liver (C) and muscle (D) of 3-month-old CONT, FIGIRKO, and F-Quint KO mice. Results represent 4-5 mice per group. E) mRNA expression of *Gys2* relative to *TBP* in liver of 3-month-old random fed CONT, FIGIRKO, F-Quint KO mice. Results represent 4-9 mice per group. Statistics were performed using a one-way ANOVA, where $*P < .05$, $**P < .01$.